EVALUATION OF CONNECTIVITY INDICES APPLIED TO A MEDITERRANEAN AGRICULTURAL CATCHMENT

Janet Hooke[1],

[1]School of Environmental Sciences, University of Liverpool, Roxby Building, Liverpool, L69 7ZT, UK;

Corr. Author; email: janet.hooke@liverpool.ac.uk

Jonas Souza[2],

[2]Geoscience Department, Center for Exact and Natural Sciences, Paraiba Federal University, João Pessoa, Brazil.

Miguel Marchamalo[3],

[3]Tech Univ Madrid, Dept Land Morphol & Engn, ETSI Caminos Canales & Puertos, Madrid 28040, Spain

Abstract

Connectivity analysis has proved a very valuable approach in understanding runoff and sediment fluxes in catchments. Many analyses use Connectivity Indices to model the patterns, but various versions of the Index have been developed. This paper tests the effects of these variants of the Index as applied to an agricultural-terraced catchment in the semi-arid Mediterranean region where occurrence of connectivity is relatively well documented to validate the modelling. This paper compares three versions of the Connectivity Index that use vegetation/land use (C), topography (RI) and roughness (n) as the weighting factors. Two different slope algorithms are also tested. The weightings are derived from a UAV (drone) survey, with simultaneous ground field mapping. The UAV imagery is found to provide a good, high resolution basis for determining detailed topography and vegetation cover. The slope limit present in some modelling is found to be unsuitable in this

landscape where steep terrace embankments that are vegetated in places, and also partially vegetated uplands, occur. Subsequent modelling removed the slope limit. The major patterns of flow produced are similar between the models and are largely related to the overall topography and major drainage lines but considerably modified by the terracing. The model outcomes differ in detail, with the C factor model, incorporating vegetation, coming nearer to the field situation. The main deficiency in all the indices is the weakness in modelling ponding and sedimentation created by the terraces, and therefore the disconnectivity in the landscape. Comparison with field data confirms the variable connectivity in rainstorms, the effects of features such as tracks, and the effect of management actions. Evidence from field mapping during the last two decades indicates that the models probably represent the maximum possible functional connectivity.

Key words: Connectivity Index; vegetation; soil erosion; sedimentation; drylands; disconnectivity

1. Introduction

The concept of connectivity has received increasing attention in hydrology and geomorphology since the late 1990s and is now widely accepted as a major paradigm and framework for analysis of runoff and sediment flux in catchments and the effects of various characteristics. It has been shown to be of value in assessing sources of sediments, soil erosion distribution, sediment delivery and sediment yield and has been applied in catchment and river channel management (Brierley et al., 2006; Fryirs et al., 2007b; Wohl et al., 2019). The main conceptual developments, building on the original ideas and applications by Brierley and Fryirs and associates (Brierley and Fryirs, 1999; Fryirs and Brierley, 1999), refined ideas on controls of connectivity and identification of connected and non-connected or disconnected areas (Bracken and Croke, 2007; Bracken et al., 2013; Lexartza-Artza and Wainwright, 2009; Wohl, 2017). States of structural and functional connectivity were differentiated and different

types of connection of longitudinal (downslope, down channels, hillslope- channel coupling), lateral (channel- floodplain) and vertical (within soil layers and water bodies) were identified (Lexartza-Artza and Wainwright, 2009; Wohl, 2017) . The importance and types of disconnectivity have been recognised (Fryirs et al., 2007a; Hooke, 2003; Hooke and Sandercock, 2017; Recondes, 2017a; Sandercock and Hooke, 2006).

The idea that not all sediment eroded in a catchment is delivered downstream has long been recognised in the concept of Sediment Delivery Ratio (Walling, 1983), in the jerky conveyor belt concept that included storage (Ferguson, 1981; Newson, 1997) and was demonstrated in sediment budgets produced by Trimble (1983). Connectivity was distinctive in concentrating on the pathways and the extent of links between potential sources and sinks all the way through the flow and sediment routes, rather than lumping catchment characteristics and quantifying outcomes from areas. Various approaches to quantification of connectivity have been developed but the breakthrough came with the Index of Connectivity (IC) developed by Borselli, et al (2008), which has formed the basis for much subsequent modelling. The IC was further elaborated by Cavalli and associates, using some different factors and weightings (Cavalli et al., 2013). Transformation of the calculation of Index of Connectivity (IC) for areas into an accessible software package opened up application by the research community (Crema and Cavalli, 2018). Alternative approaches to quantification include use of graph theory and network parameters (e.g., Fressard and Cossart, 2019; Heckmann and Schwanghart, 2013). Increasing availability and resolution of remote sensing imagery and techniques of spatial data acquisition have facilitated the development and application of connectivity concepts and quantification (Cantreul et al., 2018; Cavalli et al., 2019). Many of the applications and analyses of the Borselli/Cavalli Indices of Connectivity have been in either mountainous environments, with emphasis on rocky hillslopes and zones prone to debris flows and landslides (e.g., Bordoni et al., 2018; Persichillo et al., 2018; Schopper et al., 2019; Scorpio et al., 2018; Zanandrea et al., 2019) or in Mediterranean agricultural environments where agricultural terraces and land use influence patterns of connectivity (e.g., Calsamiglia et al., 2017; Calsamiglia et al., 2018a; Lizaga et al., 2018; López-Vicente and Alvarez, 2018), though

applications are rapidly expanding to a wider range of climatic, topographic and land use environments.

The connectivity indices developed by Borselli and Cavalli use characteristics of each pixel of a catchment or study area to calculate the potential for flow connection and cumulate this in the downslope direction, producing maps of the values of the index for every pixel. The Connectivity Indices are increasingly used to test the effects of various factors and changes such as in land cover or presence of structures (Cucchiaro et al., 2019; Kumar et al., 2014; López-Vicente et al., 2017). Various researchers have experimented with introducing additional factors and weightings to calculate the index and have suggested modifications, especially for lowland and more vegetated environments (e.g, Gay et al., 2016; Zingaro et al., 2019). However, here the three main models of Borselli (C factor), and Cavalli (n and RI versions) will be tested since they are in widespread use but still require greater evaluation, especially against field observations. All the indices aim to model the pathways of flow that will occur given the conditions of each pixel and to quantify the cumulated amount of flow and sediment but use weighting factors to assess the influence on sediment transfer. Factors that contribute to the index are flow surface controls, such as topography elements and surface roughness, represented by land cover (Borselli et al., 2008; Cavalli et al., 2013; Surian et al., 2016). The models have differing emphases, through different factor weightings, on the topographic and vegetation elements, reflecting the environments for which they were developed. Borselli's was developed for Mediterranean upland agricultural environments, including specifically partly in the present study catchment (Recondes, 2007b). Cavalli's indices were developed for steep rocky terrain as found in the Alps.

Deficiencies in the connectivity indices have been recognised (e.g., Heckmann et al., 2018; Wohl et al., 2019) and several researchers emphasise the importance of field mapping for validation and for verifying actual existence of pathways (Cossart et al., 2018; Messenzehl et al., 2014; Nicoll and Brierley, 2017). Recent research is assessing the effectiveness of use of drones for validation and/or

DEM creation and is testing effects of DEM resolution (Cantreul et al., 2018; Estrany et al., 2019; López-Vicente and Álvarez, 2018; Tarolli et al., 2019).

The main purpose of this paper is to assess the suitability of connectivity indices to characterise patterns of flow and sediment connectivity in Mediterranean, agricultural terraced landscapes, validating this approach on a previously mapped area where much is known on patterns of connectivity. The aim is to assess the extent to which connectivity indices allow modelling both of flow and sediment fluxes and connectivity adequately and to evaluate the influence of factors that are under-represented or underestimated. This will lead to suggestions of strategies for improvement and applicability of IC models. A secondary aim is to assess the efficacy of use of drone imagery for mapping connectivity and calculating indices. The paper also highlights the challenges of validation, the effects of changes over time, and the high degree of human influence in such a landscape.

2. Methods

2.1 Study area characteristics

The area used for this testing and evaluation of connectivity indices and drone deployment is a sub-catchment of the Cárcavo catchment in SE Spain (Fig.1), which was the location for most of the work on development of connectivity assessment and effects of vegetation undertaken in the EU RECONDES project (Hooke and Sandercock, 2017, 2012; Marchamalo et al., 2016; Recondes, 2007b; Sandercock and Hooke, 2006), including research by Borselli and colleagues on development of their index. The area has an average rainfall of c.300 mm/year and the whole catchment is mainly underlain by Miocene marl. The selected sub-catchment has an area of 14ha and the main drainage is in the northeasterly direction (Fig. 1), with a total relief of 46 m. It is an area of mainly terraced almond and olive groves but contains some abandoned land and areas of rock outcrops with semi-

natural vegetation and of afforestation on the margins (Fig. 2). It has one main track crossing it and the remains of another old, abandoned track, and also ramps for access to fields between terraces. The relief or banks between terraces are of the order of 0.5-1.5m in height, with varying degrees of vegetation cover (Fig.2). The fields with almonds and olives are ploughed frequently, usually about three times a year. Some fresh planting of trees in terraces has taken place over the past 10 years, mainly for replacing dead trees. Vegetation on embankments and in the semi-natural areas is not highly seasonal, comprising mostly perennial shrubs that withstand drought and alter very little year to year or seasonally. Ground cover of herbs can appear after wet periods but is mostly soon removed by ploughing. The area has been monitored by field mapping since 2004, with frequent mapping in the period 2004-7 (a dry period) and sparse surveys, mostly annually in January, since then. The major connectivity patterns and their relation to rainfall have already been analysed for the early period (Marchamalo et al., 2016).

Fig. 1 - Cárcavo location, relief and land use

The major characteristics of the connectivity pattern revealed by the mapping 2004-7 (Marchamalo et al., 2016), and confirmed in subsequent mapping, are summarised here (Fig. 3). The main drainage lines correspond to the overall original topography of the catchment, with central flow to the north-east down the centre of the area but modified by the terracing and management actions. Mapping after rainfall events, varying in magnitude but mostly low magnitude and at differing times after management actions such as ploughing (but mostly in the same season of January), shows that a major feature of the drainage and connectivity is the occurrence of relatively short pathways in storms, that are erosive, producing rills, but that most of these usually terminate in areas of ponding and sedimentation upstream of the terrace embankments (Fig. 2c). Breaches in the embankments or overflow/ throughflow have occurred in high rainfall events, though rarely (Fig. 2c). Management actions have directly altered the configurations in some locations, with the main natural drainage

being slightly shifted into a constructed ditch in the lower section (Fig. 2a), a minor track crossing put in at the head of the main gully at the downstream end, and some large soil piping (tunnelling) in fields upstream of the main gully/channel (Hooke, 2006; Hooke and Sandercock, 2012; Marchamalo et al., 2016), in existence until 2011 then filled in (Fig 2a). The previous analysis had shown that the main track crossing the area in the upper part is highly influential in generating runoff Fig. 2c), as is also an abandoned former agricultural area of low vegetation cover (Fig. 2a) (Hooke, 2006; Hooke and Sandercock, 2012; Marchamalo et al., 2016). Regular maintenance actions include mending of breaches, frequent ploughing and weed control, and replacement and replanting of trees in some fields.

2.2 UAV survey, and DEM construction

A DJI Phantom 3 was used to take aerial photographs of the sub-catchment, in January 2019; the flight was operated at 60 metres high, 75% of frontal and lateral overlapping, and it took 265 photos. All images had UAV natural 3D georeferenced information. Nevertheless, 13 ground control points were established at different altitudes around the watershed, with the markers surveyed using a Topcon GPS RTK HiperPro instrument with <20 mm error. The UAV data were processed in Agisoft Metashape Professional, including the spatial adjustments based on the ground control points and a two-step, no ground points filtering, to remove vegetation and man-made structures. It was possible to create DEMs with different resolution but in this analysis only the 0.2 m spatial resolution DEM was used, following conclusions by López-Vicente and Álvarez (2018)**,** working in a Spanish Mediterranean agricultural terraced area similar to the present field area, in which they specifically tested different DEM resolution from drone images. They concluded that 0.2m DEM provided the best IC result, vertically and horizontally, including good results to identify the small erosion lines, that are around 0.2m wide, like those found in the Cárcavo area. Our preliminary tests of different resolutions confirmed these findings. Ground photographs and field mapping were undertaken at

176 the time of the drone photography. In addition, an orthophotomosaic with 0.03 m spatial resolution
177 was created, and together these allowed connectivity ground truthing.
178
179 ***2.3 Calculations of indices and series of tests***
180 One of the frameworks that allows quantification of the connectivity is the Index of Connectivity (IC)
181 (Borselli et al., 2008), that calculates the continuous potential connectivity between different points
182 on the surface. The IC uses a GIS model approach to define the potential connectivity on a pixel/cell
183 scale. It combines a downslope component and an upslope component (Equation 1). The downslope
184 component (D_{dn}) is related to the distance and impediments between a point and the nearest sink.
185 These downslope impediments are defined by the cell slope angle (S) and the cell surface roughness,
186 defined by vegetation and land use characteristics (Borselli et al., 2008; Sougnez et al., 2011),
187 classified as the Weight factor (W). The W value ranges between 0 and 1, higher values representing
188 less roughness and consequently higher connectivity. The upslope component (D_{up}) is based on
189 potential runoff/discharge, calculated by discharge area (A), and on sediment yield potential,
190 controlled by upslope average slope angle (S) and upslope average surface roughness (W). It is
191 expressed by:

$$\mathrm{IC}_k = \log_{10}\left(\frac{D_{\mathrm{up},k}}{D_{\mathrm{dn},k}}\right) = \log_{10}\left(\frac{\overline{W}_k\ \overline{S}_k\ \sqrt{A_k}}{\sum_{i=k,n_k}\frac{d_i}{W_i S_i}}\right)$$

192 (Equation 1)

193 In the Borselli et al. (2008) model the W is related to the C-factor used in USLE/MUSLE models; this
194 parameter reflects soil protection and soil loss (Table 1). Also, it is possible to include several
195 sediment sinks, such as streams, roads, urban areas (Borselli et al., 2008) or the watershed outlet
196 (Cavalli et al., 2013). In this paper, to understand the whole watershed connectivity pattern, the
197 lowest downstream point of the main drainage area studied was defined as the outlet and used as
198 the sink target.
199

200 *Table 1*

201

202 Cavalli et al (2013), made three relevant changes to Borselli's IC in their original model, termed the
203 RI model because it incorporates a roughness factor model: flow direction algorithm changed from
204 D8 to D-infinity to allow for divergent flow paths; created a slope angle limit; and changed the C-
205 factor to a topographic roughness index (RI). The authors made clear that changes were necessary
206 due to the specific mountainous rocky surface they were analysing and to the possibility to use high
207 resolution digital terrain models (HR-DTM). The D-infinity algorithm enables identification of
208 divergent flow dynamics and, as a result of DTM cell size, it could identify more accurately the flow
209 width than the D8 algorithm, which identifies only one flow direction, neglecting divergent flow
210 patterns and the flow width (standardised as the pixel width). The slope gradient limit was set as 1
211 m/m in the Cavalli model, justified by the local characteristics in their analysed area, where areas
212 with gradient over this limit show no or very little sediment availability, such as rocky cliffs, very
213 steep slopes and bedrock channels. The third, and critical change, was the replacement of the C-
214 factor by RI derived from the HR-DTM, using a 2.5 m DTM. The reason for this modification is the
215 lack of vegetation and land use in the mountainous/Alpine area, where the surface roughness is
216 controlled by surface morphology of rock outcrops and debris cover. The RI parameter (Cavalli et al.,
217 2013) is the standard deviation of the residual topography (x_i-x_m) (Equation 2) and it is defined as
218 the Weighting factor (Equation 3) following the expressions:

219

$$RI = \sqrt{\frac{\sum_{i=1}^{25} (x_i - x_m)^2}{25}}$$

220 (Equation 2)

$$W = 1 - \left(\frac{RI}{RI_{MAX}}\right)$$

221 (Equation 3)

Additionally, the authors indicate that this allows the model to run with only one input data, the residual topography, turning this IC-RI model into the most commonly used (Calsamiglia et al., 2018b; Cantreul et al., 2018; Marchi et al., 2019; Messenzehl et al., 2014; Nicoll and Brierley, 2017; Schopper et al., 2019), especially after the release of a free open-source tool – SedInConnect (Crema and Cavalli, 2018). Subsequently, vegetation and land cover data were re-introduced as W, based on Manning's n roughness coefficient (Bordoni et al., 2018; Persichillo et al., 2018; Surian et al., 2016), following the idea to use RI for unvegetated areas and Manning's n roughness coefficient for vegetated areas (Table 1). There are several other approaches to calculate the connectivity index at cell scale using different Weighting factors, such as NDVI vegetation index or other environmental parameters (Cislaghi and Bischetti, 2019; de Walque et al., 2017; Gay et al., 2016; Ortíz-Rodríguez et al., 2017; Zingaro et al., 2019).

Initial models were run in the present research to test the difference between the index calculation using no slope restriction, as in Borselli et al. (2008) (subsequently denoted here as Bor_IC) and using the restriction in the Cavalli model of a slope limit of 1m/1m (denoted as Cav_IC). In the Cárcavo environment, there are steep slopes that are not rocky, mainly embankments with varying degrees of vegetation. At the same time, the three main weighting factors were used – C factor (C), Manning Roughness Coefficient (n), and Topographic Roughness Index (RI) to test the differences produced by those factors. The land cover map was created using the UAV orthophotomosaic and field data, identifying the vegetation cover and land use and soil management. The C-factor values and Manning coefficient values applied (Table 1) were based on well-known values in the literature (Panagos et al., 2015; Papaioannou et al., 2018; Persichillo et al., 2018). The RI was calculated using the 0.2 m UAV DEM in the SedInConnect tool (Crema and Cavalli, 2018). The D-infinity algorithm, proposed by Cavalli et al. (2013) was used, because it is widely regarded as a better algorithm than D8 (Lana-Renault et al., 2018; López-Vicente and Álvarez, 2018; Messenzehl et al., 2014; Nicoll and Brierley, 2017; Ortíz-Rodríguez et al., 2017; Persichillo et al., 2018; Schopper et al., 2019).

It is essential to understand the complexity of comparing the different versions of IC models, mainly changes in W parameters (e.g. C/n from land use and RI from topographical information). These W values do not show a similar histogram value distribution (Fig. 4), leading to unequal values that are not directly comparable. Because of this characteristic, using absolute thresholds to compare different unnormalised models creates misinterpretations. As a result, IC model comparisons use different statistic distribution analysis methodologies, such as stretch distribution (Chen et al., 2013; Estrany et al., 2019; Zhao et al., 2020; Zingaro et al., 2019); data clustering visualisation (López-Vicente and Ben-Salem, 2019); and percentile thresholds (Calsamiglia et al., 2018b; Calsamiglia et al., 2020). The results here were classified using Jenks natural breaks (Persichillo et al., 2018; Tiranti et al., 2018) in 10 classes. This data clustering method aims to find the optimal arrangement of classes by minimizing the average deviance from each class mean in distributions that do not show obvious natural/fixed breaks (Chen et al., 2013). These classes were grouped into three divisions of Low connectivity (classes 1 to 3), Moderate connectivity (classes 4 to 7), and High connectivity (classes 8 to 10) for spatial visualisation of the IC maps.

2.4 Field mapping methods and dates.

Field mapping of connectivity was undertaken by ground walk-over surveys, observing and measuring signs of flow lines, erosion and deposition, and marking them on a base map, supplemented by GPS points and photography to record features (Marchamalo et al., 2016). Connectivity pathways are followed and interpreted in the field at the time. The base map used was a 1/5000 map produced from orthophotos by Murcia Region (1995). The field mapping was undertaken using the protocol developed in the RECONDES project (Cammeraat, 2005), applied by Borselli et al. (2008) in developing and testing their index, and applied in the Cárcavo catchment in studies by Lesschen et al. (2009), Marchamalo et al. (2016) and Meerkerk et al. (2009). Since 2007, it has only been possible to map the area occasionally and not necessarily after heavy rainstorms. It

274 did include mapping after the heavy rainfall and flood events of September 28th, 2012 in SE Spain
275 (Hooke, 2016, 2019) but rainfall was not extreme in the Cárcavo catchment. Subsequent to the
276 drone photography, mapping also took place in January 2020 after very heavy rain of >200mm in
277 September 2019. Frequency of repeat flow lines has been assessed (Fig. 3). The compilation for the
278 period 2008-20 only shows the main rills, for clarity. Rill lines that are not continuous usually
279 terminate in small fans or very shallow sedimentation zones (Fig. 2c). The field mapping is also
280 complemented by ground photography and field notes, including evidence of management actions
281 and alterations, major ones of which are indicated in Fig.2a.
282
283 *Fig. 2*
284
285 **3. Results**

286 **3.1 Effects of slope restriction**
287 Six models were processed – Bor_C, Bor_RI, Bor_N, Cav_C, Cav_RI, Cav_n – where "Bor" represents
288 the models without slope limit, "Cav" the models with 1 m/m slope limit; C is C-factor as W, RI is
289 Topographic Roughness index, and n is Manning's Roughness Coefficient. The effects of using the
290 Cavalli algorithm that has a slope limit of 1 m/m (45 °) were compared with the results after removal
291 of the slope limit. Steep slopes (angle over 45º - 1 m/m) represent 1.1% of the watershed, mainly
292 terrace embankments and natural hilly areas. Firstly, to identify the slope limit effects on IC models
293 (Table 2), these steep areas were separately analysed. The comparison results in the expected
294 increase in proportion of high connectivity areas in the models without slope limit ("Bor" models),
295 proportionally increasing by 0.7% (C-factor), 4.0% (Manning's roughness coefficient), and 3.4%
296 (Roughness index) for the three versions of the IC. Consequently, the different slope sensitivity of
297 the IC models is evident, where the land use parameter can decrease the influence of the slope
298 angle, notably in the C-factor model. In this case, this happens because the steep slopes are
299 concentrated on the terrace embankments and around the hills, which are predominately covered

by denser vegetation, like trees and bushes. Likewise, the roughness index will increase with the topographic variation, compensating the slope sensitivity. On the other hand, the increase of 18.6% (from 18.2 to 21.6) in the Manning coefficient is controlled by the small amplitude of the values in different land cover types (0.6 to 0.95), showing low sensitivity to the land cover parameter and enhancing the slope importance. Although slopes of > 45 ° represent only 1.1% of the total area, the results (Fig. 5) show clearly there is an impact on the connectivity at the embankments. The slope limit can mask high connectivity areas on the embankment, that can generate erosion and embankment failure and alter connectivity pathways significantly (Fig. 2c). The justification given by Cavalli et al. (2013) for this limit (that when there is more than 45º there is only rock exposure) cannot be applied to this area, therefore the subsequent analyses are carried out with the models without slope limit.

Fig. 5

3.2 Comparison between connectivity models and with field evidence

Subsequent IC modelling has been carried out for the three versions of the indices, Borselli C factor (IC_C), Cavalli Manning n (IC_n) and Cavalli Roughness Index (IC_RI), all without slope restriction. They have been applied to the whole catchment and to five sub-areas that represent different types of terrain and land use as follow (Fig. 6):

1. Whole catchment
2. Runoff from upland, area of abandoned land leading to a culvert under track and into terraced almond groves
3. Part of rocky, steep, semi-natural area with scrubby vegetation
4. Main cultivation area with division into strips, terraced with vegetated embankments
5. Main strip field areas, separated by embankments, different types and conditions of trees.
6. Zone of high relief agricultural terracing in former central main drainage line.

For each area, a comprehensive analysis has been carried out, integrating the drone imagery, the slope values, the IC outcomes using the C, n and RI factors, and vectorial features mapped from drone imagery (Figs. 6-10). The patterns of flow predicted by the indices are also compared with the longer-term field mapping records, both from 2004-7 (Marchamalo et al., 2016) and 2008-2020 (Fig. 3), and the 2019 field mapping at the time of the acquisition of imagery, and with all field notes and ground photography of every date. The comparative statistics for proportions of area in each grouped connectivity class for each model version for the whole catchment and the selected sub-areas are presented in Table 3. The results, comparing the models and also comparing with field evidence, for each of these areas are summarised in the following sections:

1. **Whole sub-catchment (Fig. 6).** Large differences emerge using the Borselli index C-factor compared with n and RI. In the C model, zones of low connectivity are all the fields and most slopes. High connectivity areas are the edge of the upland in the south and the gully head and main channel at the downstream end (North end of image). RI and n produce much more extensive areas of high connectivity. The high connectivity areas (implying major sources) are mostly the bare areas but also low vegetation areas at the base of the uplands and the steeper areas near the main gully/ drainage head, though vegetation cover is high in parts of that. Threads of channels show up on all sets but are much more obvious on n/ RI versions. They do show some flows through/ over embankments. The main drainage lines, influenced by topography, do emerge strongly in all models. Uplands themselves emerge as low connectivity on C maps but higher in n and RI models. Lateral flow in terraced fields is present to a limited extent but does not emerge as a strong element. In relation to field mapping over the longer term, almost all fans mapped in the field are omitted and flow is shown as more continuous than actually occurs on most occasions.

Fig. 6 Whole catchment model.

2. **Artificial pipe (culvert) and track area (Fig. 7)**. For all three versions, the IC outputs show some major drainage lines present, with similar pattern and replicating the culverted flow under the track. The prominent patterns are of two main drainage lines crossing the track and one ancillary flow from the SE. The main flow from upstream of the track, which is from the bare area of abandoned land above that does actually occur frequently, is correctly predicted and corresponds to where the culvert now leads flow under the track. Relatively high generation from the track is correctly simulated by the C model but much lower connectivity is shown in this zone on the n and Ri models. The more southerly flow line has not been observed to cross the track but flow is often generated from the track. The main flow downstream of the track in all the models replicates the long existing and highly frequent rill present there after most storms (Fig. 3). The SE flow appears from the photographs and in the field to be highly influenced by the plough lines at the time of drone imagery, which is a recurrent situation in the field. The flow lines are conditioned by this pre-existing topography, including the persistent rills, and the presence of the culvert. Overall, the modelling picks up some of main lines but some of the links differ in detail from the field mapping. The C-weighted model differs from the n and RI in degree of connectivity of the low gradient, bare ploughed fields downstream of the track. The statistical distribution of IC values for each version indicates that the area has a generally low proportion of high connectivity, but it is much higher for the C model than n and RI models. The large differences are in medium connectivity, rather than low connectivity.

Fig. 7

3. **Natural area and main track (Fig.8).** Very large differences in degree of connectivity and intensity of flowlines northwards off the upland are apparent between the models. The

connectivity is low for the C factor model, but that model shows high connectivity at the base of the upland to the north, which is an area of abandoned land with little vegetation and a resistant surface. All three factors indicate the exit of the flow in the same location which is a pre-existing breach (X). All three versions produce a small distinct drainage in the SE corner, which did actually occur as a major flow down an old, minor track in 2020 after the heavy rain of September 2019, and with large deposits formed at the end of the old track onto the main track. Only minor flows and rills were visible prior to that. All model versions show a slight flow off the downslope side of the main track which has occurred occasionally. Overall, the connectivity pattern mostly comprises short paths in the field, which are picked up to some extent by the models, but some extra pathlines, never observed, are modelled. The statistics indicate much higher connectivity for RI than C and n models. The upland area is steep and rocky with relatively dense vegetation cover; it is not very erodible and supplies little sediment.

Fig. 8

4. **Terrace lines (Fig. 9).** The main drainage lines are similar between the three models but vary in intensity. All show the main drainage line flowing east near the W-E field boundary which has always been a major flowline and was converted into a major ditch in late 2011. The Index maps do not detect the exact position of that correctly but do show the natural rill that frequently develops down the ramp and was the former main drainage (Y) (Fig. 9). All three models show zones of high connectivity and potential source areas just downstream of the N-S embankments, influenced by the steep slopes, although to differing degrees between the two main zones. These are not obvious source areas in the field and are influenced by the blockage effect of the embankments. All models show a flow through the easterly embankment which is a pre-existing breach (Z) but the soil piping leading to it was filled at the time of the ditching in 2011. They also show the flow diagonally across the NE field which was a line of deep soil piping (Hooke, 2006; Fig. 2) until filled by the farmer in

2015, though it partially reopened in the very big storm of September 2019. This is the line of natural drainage influenced by the overall topography. Some minor parallel rills in the southernmost field are picked up by the models. The statistics reveal that the proportion of low connectivity is markedly less in the C factor model, that shows the vegetation connectivity buffering effect in the fields. The proportions of high connectivity are similar for all three outputs, but the contributions of these source zones are different between the three models.

Fig. 9

5. **Terrace area (Fig. 10).** All model versions pick out differences between the different fields which are due to varying cover and recentness of ploughing, but this is much more distinct on C factor model maps. All pick out the drainage lines parallel to the field boundaries and the lines of ploughing. In this area, the terraces are levelled up by embankments but the overall slope is to the north. A few breaches by northerly flow in the southerly embankment are indicated on the n and RI maps, which are rarely present in the landscape. A bank failure on the northerly embankment is not influencing the flow lines, nor has it in field mapped activity. The vegetated embankments themselves are zones of low connectivity on all models. The whole area is modelled as of low connectivity and field mapping also detected little activity throughout the period (Fig.3). It was only in the 2006 event and to some extent the 2020 event that longer rills and extensive sedimentation were visible, parallel to the embankments. The statistics confirm the high proportion of low and medium connectivity areas for all versions. However, the distribution between low and medium is very different for C from n and RI models, with the former having much greater medium connectivity, reflecting the influence of the differing vegetation covers.

Fig. 10

6. **Central drainage area (Fig. 11).** This is a complicated area in the main topographic drainage zone, but with two sets of highly vegetated steep embankments influencing the flow lines.

All three index maps show two main flow lines, one from the southern field flowing east of the central vegetated bank and the other flowing from the westerly field through the gap in the embankment then round the vegetated zone. Both these flow lines have occurred in the field, though the former was only detected in 2019 and 2020, becoming much more active in recent years. The index maps fail to show the flows linking up to some extent and they fail to show the sedimentation area. Indeed, on the n and RI model maps what was observed to be a sedimentation zone and fan area in the field is marked as a high connectivity, source zone. This area was heavily influenced by tractor wheelings in 2019 so some rills that must have produced the sedimentation had been flattened or are not clearly visible on the drone imagery. The flow over the W-E bank in the centre is picked up by all three models. All three outputs showed similar proportions of high connectivity areas, but the medium connectivity area proportion is much higher for the C model and lower for low connectivity than in the n and RI models. Overall, the models are replicating well the complicated patterns of flow in this zone, but they are determined to some extent by the rills and flow lines detected by the drone photography and DEM and so are reproducing these patterns. The C model represents better the low connectivity on vegetated embankments, while the n and RI models over-estimate these areas, showing high connectivity on the conserved embankments.

Fig 11

Overall, the modelling does not pick up major lines of flow parallel to field boundaries adequately, nor the position of all breaches that have occurred at times of high runoff. The models in general do not detect fans and major areas of ponding and sedimentation that occur in many events and thus zones of disconnection, at least for sediment. All the models reproduce most of the major drainage lines.

4. Discussion

Conclusive results were obtained on the effect of removing the slope limit for this type of Mediterranean terraced landscape, that was introduced in the Cavalli versions of the model. The tests showed clearly the impact of the slope limit on the connectivity at the embankments. The slope limit can mask high connectivity areas on the embankment, that can generate erosion and embankment failure, as observed in the 2006 flow event (Marchamalo et al., 2016). It may also be why, for example, Calsamiglia et al. (2018a) identified that 27% of their terrace embankment failures happened on medium and low connectivity points, with no clear signal of flow lines.

Comparison of the outcomes of the three different versions of the IC model, using the same input data of the DEM and at a resolution of 0.20 m and using no slope limit, predict largely the same overall major drainage lines and the statistical results indicate similar proportions of areas in different connectivity classes (Table 2). A relatively low proportion of the total area shows high connectivity but the values provided by the models vary from 9.5 % (n) to 14.6% (C factor). The differences in connectivity proportions are largest in area 2, draining some low-gradient, abandoned land and the main track, with the C-model giving a higher proportion of high connectivity. In the other areas (areas 4, 5 and 6) which are mainly agricultural terraces, the C factor model tends to distribute more of the area into the medium connectivity category than low connectivity compared to the n and RI models, but proportions of high connectivity are similar. In the upland zone (Area 3), which is steep but vegetated, the RI index gives much more high connectivity, and the C factor model produces more low connectivity area.

Thus, some of the most notable differences between the models are in areas where the RI and n models are not detecting the effects of dense vegetation, e.g. on embankments, or cover in fields and on the rocky slopes. In the indices, RI and n only have a limited range of values, mainly related to topographic influences, whereas weighting using the crop factor provides a much greater range of

478 values (Table 1) and allows for different cover modelling and is thus more sensitive. Experiments
479 were undertaken with using absolute values and the same class thresholds for all models but this
480 misrepresents the modelling. It is also unknown which model to standardise onto unless field
481 validation is undertaken. Therefore, we have used relative classes. Other researchers have compared
482 different scenarios using absolute values in a specific model but not comparison between models.
483 The present models produce a high density of flow lines, probably representing maximum potential
484 connectivity under prevailing conditions and structures. The grouping of the 10 connectivity classes
485 into three clusters (low, medium and high connectivity) helps to clarify the patterns and identify
486 main pathways more easily.

487

488 Vegetation cover on the embankments has been identified from the field mapping as limiting
489 connectivity. On the other hand, vegetated banks have steep slopes, enhancing connectivity. The
490 degree of vegetation cover and nature of the embankment is important and not well modelled by
491 the n and RI models. Vegetation effects do include a roughness influence, which decreases velocity
492 and thus erosion , but vegetation also increases resistance to erosion and increases infiltration, so
493 decreasing runoff (Hooke and Sandercock, 2012; Sandercock and Hooke, 2011). It has been shown
494 in this catchment and in other locations in SE Spain and similar landscapes that embankment
495 breaches are often the initiation point of gullying in abandoned lands, where embankments are not
496 maintained, (Faulkner, 2008; Hooke and Sandercock, 2012; Lesschen et al., 2008, 2009). It was a
497 recommendation made in the RECONDES study on use of vegetation to combat land degradation
498 (Hooke and Sandercock, 2017, 2012; Recondes 2007a, 2007b) that embankments and ramps
499 between terraces should be vegetated to reduce connectivity. Hooke and Sandercock (2012, Fig. 9)
500 used the present study area to illustrate how strategies of use of vegetation to minimise connectivity
501 and reduce soil erosion could be applied. This also has important implications for conservation
502 agriculture and restoration in degraded lands of the world, where vegetated bunds can be highly
503 effective in reducing runoff and erosion.

504

505 The other major deficiency in all the tested connectivity indices is that they do not work well in flat
506 land and, very importantly, they do not adequately map areas of ponding, infiltration and sediment
507 deposition, or some flow lines parallel to field boundaries found in these terraced landscapes (López-
508 Vicente et al., 2013; Calsamiglia et al., 2018a; Moreno-de-las-Heras et al., 2019). On many of the
509 terraces in the field maps, it can be seen that flow and sediment go into sink areas as small fans at
510 the end of the terrace, and flow paths do not cross into the next terrace, or only do so on rare
511 occasions of high rainfall amount (Fig. 12). Some of the fan/ deposition areas are shown as major
512 source areas in the modelling, rather than stores/ sinks, implying that they overflow, which is not
513 always the case. That could result from the DEM 0.2m resolution that identifies even tiny rills,
514 overestimating the connectivity process generated by these features, creating non-existent source
515 areas. Field observations confirm that these flat sedimentation areas act as disconnectors for most
516 frequent storms and very few connect up even in the larger storms (Marchamalo et al., 2016),
517 including the 200mm storm of September 2019 (Fig.3b), so it is difficult to identify thresholds for
518 overflow. The formation of terraces has a major aim of creating ponding, increasing soil moisture
519 retention and decreasing soil loss, which can be seen in several studies (Calsamiglia et al., 2018a;
520 Calsamiglia et al., 2018b; López-Vicente et al., 2013; Moreno-de-las-Heras et al., 2019). They have a
521 major effect on connectivity, which is not being adequately predicted by the models. This is partly
522 because the algorithms in the IC models use conditioned hydrological DEMs to create flow
523 accumulation and downstream length parameters. They remove spurious sinks and wipe out natural
524 depression and structural disconnection on erosion/drainage lines. On the other hand, they may be
525 representing the maximum possible potential of connectivity. Cantreul et al. (2018) show that small
526 feature responses are directly affected by pixel size, larger pixel sizes hiding the connectivity effect.
527 At the same time, several studies do identify structures such as roads and tracks as decoupling
528 elements (Calsamiglia et al., 2018a; Kumar et al., 2014), and the original model used roads and
529 paths as disconnectivity structural element (Bordoni et al., 2018; Borselli et al., 2008). It is possible

530 to produce temporary sinks by inserting depressions and disconnectivity elements in the models as
531 polygonal "zero" values but this has mostly been done for the large features and structures such as
532 roads, lakes and check dams. (Bordoni et al., 2018; Borselli et al., 2008; Franco and Souza, 2019; Gay
533 et al., 2016; López-Vicente et al., 2020). The software for the calculation of the Cavalli index does
534 now have an option to input sinks into the DEM/ surface conditions
535 (https://github.com/HydrogeomorphologyTools/SedInConnect_2.3/) but these are pre-determined
536 by the user and therefore it does not independently predict where storage will occur. Pre-entering
537 where sinks are located from field evidence negates the value of use of the IC modelling as a
538 predictor.
539
540 The adequacy of the models to predict soil erosion and sediment flux at this scale is debatable.
541 Although the models demonstrate a sensitivity to micro-topography, which has been shown to be
542 highly influential in several studies from field observations (Sampson et al., 2012), IC models do not
543 adequately model the differing nature and erodibility of the surfaces, particularly infiltration
544 capacity and surface resistance, Thus, the effects of harder surfaces such as tracks are
545 underestimated. Tracks have been shown to be very high generators of runoff in many landscapes
546 (e.g. Croke et al., 2005). The IC maps are displaying the potential runoff pathways, but they do not
547 indicate which are erosive and therefore the formation of rills and gullies and potential removal of
548 soil and transfer downslope. It is assumed in the modelling that erosion and sediment fluxes are
549 proportional to the connectivity index value. Comparison of the field and drone mapping (e.g. in Fig.
550 11.6) with the model maps (Fig. 11.3-5) indicates that the main rills do correspond with high
551 connectivity lines mapped but not all lines in the model are erosional and rills. The upland areas,
552 although with steep slopes and relatively sparse vegetation, produce relatively little sediment
553 because of their resistance, whereas the bare soil areas are very prone to rilling and gullying. It is
554 therefore difficult to establish thresholds for sediment flux without ancillary information. The
555 modelled high connectivity pathways probably do indicate the potential positions of erosion or

556 supply, but the erodibility of the surfaces needs to be incorporated. Developments are taking place
557 that incorporate such factors (e.g. Chartin et al., 2017; Gay et al., 2016; López-Vicente and Ben-
558 Salem, 2019; Zingaro et al., 2019), but they require adequate data on surface material properties.

559

560 The state of the ground in 2019 obviously became the basis for the calculation of the connectivity
561 from the drone imagery, so the modelling is controlled by pre-existing features, even to the scale of
562 rills and plough lines. The influence of minor variations in topography and morphology emerges
563 clearly here and has been shown previously from field evidence to have a profound influence on
564 pathways, for example, small breaches, low points on tracks or embankments (Hooke and
565 Sandercock, 2012, Fig. 2c; Marchamalo et al., 2016). Here, the modelling replicates some effects but
566 not all subtle effects and exact locations. The extent to which temporary or ephemeral features such
567 as plough lines should influence the modelling will depend on the purpose and whether such
568 structural controls are likely to persist.

569

570 Comparisons with field mapping from less intense events, documented in Marchamalo et al. (2016)
571 and in subsequent field mapping (Fig. 3), indicate that discrepancies associated with the IC modelling
572 are not simply that the latter represents very high flows or, indeed, only detects lesser flows.
573 Marchamalo et al. (2016) have already shown that antecedent soil moisture and vegetation cover
574 conditions, as well as degree of ploughing, make a significant difference in flow and sediment
575 processes measured in the field. Major storms in September 2012 (61.3 mm in 24hr) and September
576 2019 (162 mm in 24 hr) did not, however, produce major changes or new features as expected. The
577 major exception of a new feature detected in January 2020 was a major flow and deposit from an
578 old track fringing the southern side of the upland, which was present in the models (Fig. 8) In
579 addition, the former line of large soil piping at the downstream end of the major drainage, which
580 had been filled in, was partially opened up again, which was correctly modelled, in spite of a lack of

581 topographic features in 2019 and on the DEM. The modelling therefore could provide a useful
582 indication of where deliberate modification is unlikely to be effective in high magnitude events;
583 models may show the tendency for the connectivity patterns to revert to natural drainage lines,
584 influenced by the macro-topography.

585

586 Field validation is also complicated by changes due to management. For example, over the 16-year
587 period of monitoring, connectivity has decreased in southern fields in Area 3 (Fig. 2a, Fig. 3), mainly
588 due to less maintenance and ploughing, so increased ground vegetation cover has grown in wet
589 periods, reinforcing the influence and effectiveness of vegetation cover in reducing runoff. Other
590 management actions in the monitored period include the track construction, infilling of the major
591 soil piping, and the construction of the new ditch. Tractor wheelings, ploughing intensity and
592 direction, and replanting of some trees, involving creation of pits and extra watering, have had some
593 localised effects. These are the kinds of activities common in these agricultural terraces. Overall,
594 the main lines of activity and connection have persisted, influenced by the structures, and certain
595 rills have been repeatedly reactivated.

596

597 Several researchers have used UAV imagery as the basis for connectivity modelling and detection
598 (Calsamiglia et al., 2020; Cantreul et al., 2018; Estrany et al., 2019). It has been shown here that it
599 can detect even tiny rills and plough lines so is highly effective in mapping large areas. However,
600 these will be built into high resolution DEMs derived from the imagery and the basis for the
601 modelling and therefore are bound to control flow patterns. They are not an independent validation
602 of predictive connectivity in the landscape that would take place without these ephemeral features
603 unless separate data or a lower resolution DEM is used for generation of IC. On the other hand, the
604 sensitivity of the modelling means that it could be used to detect changes produced by events or
605 management actions by altering the DEM and ground cover (Cantreul et al., 2018; Koci et al., 2020;

606 Lizaga et al., 2018; Llena et al., 2019; López-Vicente and Álvarez, 2018). Drone detection of ponding
607 and sedimentation is challenging because differences in elevation can be very small, but the
608 smoothness of the surface can be different from other areas (Fig.11, so this could be complemented
609 by spectral techniques (Asadi et al., 2019; Foerster et al., 2014; Ortíz-Rodríguez et al., 2019; Singh
610 and Sinha, 2019). However, overall, this high-resolution photography can be used for mapping of
611 features over the whole area, which is challenging to achieve in ground validation.

612

613 ***5. Conclusions***

614 Comparisons between the three main versions of the connectivity index, using C, n and RI factors,
615 for this sub-catchment in a dry Mediterranean landscape with agricultural terraces, indicate that
616 that the weight given to vegetation cover, topography and roughness effects can make a significant
617 difference to the details of the degree of connectivity, though not so much to the overall patterns
618 and location of occurrence of features. The roughness type indices (Cavalli, et al., 2013) using n and
619 RI factors underestimate the effects of vegetation, which, though sparse, can be highly influential on
620 connectivity in this type of landscape. The effects of the steepness of embankments can also be
621 underestimated if the slope limit, introduced in the Cavalli models, is imposed. Where vegetation is
622 a significant influence on runoff and erosion, the Borselli C- weighting algorithm represents the
623 connectivity more realistically than the Cavalli n and RI models. The IC indices reflect the type of
624 areas for which they were developed, but care needs to be taken in applying them to different areas.
625 Use of the C index for weighting and not using a slope limit are recommended for vegetated
626 landscapes and those with small, steep structural features.

627 Comparison with 16 years of field mapping in the area as well as the drone imagery used to create
628 the model simulations indicates that the major missing element in all the model outcomes, however,
629 is the occurrence of ponding and sedimentation on terraces and the discontinuities in pathways
630 between terraces. Modelling without considering infiltration capacity and surface erodibility

631 hinders the capacity of modelling the occurrence of erosional and depositional features, although
632 vegetation does influence those factors. The models are not dealing adequately with disconnectivity,
633 especially for sediment fluxes. Overall, the ICs are indicating flow paths and potential flow
634 connectivity, but not sediment connectivity as such, though they may show the potential for that
635 from the flow index.

636 The field mapping indicates that the modelling probably represents the maximum potential runoff
637 and all possible pathways. Grouping of connectivity classes into maps helps identification of major
638 pathways. The long-term monitoring has also demonstrated that actual responses vary between
639 rainstorms even of comparable amount, but also to more complex conditions. Some of the major
640 features created in some of the largest events are simulated by the models, although others are
641 absent. Management actions also have direct and indirect effects on the pathways in this landscape,
642 complicating the conditions and responses. Comparison of the modelling and the mapping combined
643 with effects of management actions indicate that flow is likely to revert to natural pathways dictated
644 by macro-topography in the largest runoff events.

645 The drone photography can be used for mapping major flow and erosion features but field mapping
646 on the ground is still needed. The drone imagery used for the modelling dictates the pathways
647 modelled, so presence of ephemeral features like pre-existing rills will condition the patterns.
648 However, the drone imagery also demonstrates its efficacy in providing the basis for accurate
649 modelling that detects micro-topographical variations, such as on trackways, which make a
650 difference to prediction of the location of pathways.

651 Overall, this analysis implies that the modelling cannot be used as an exact predictor, but as a more
652 general indicator of degree of flow connectivity and main pathways. It has been shown that the
653 weighting of factors in the different versions of the IC models makes a significant difference to the
654 model outcomes especially for vegetated areas. The main drawback of IC models is that
655 disconnectivities and sediment flux are not adequately modelled.

656

657 **Acknowledgements**

658 JMH and MM did not receive any specific grant from funding agencies in the public, commercial, or
659 not-for-profit sectors for this research. The funding for the original research in Cárcavo catchment,
660 2004-2007, the RECONDES project, was provided by the European Commission, Directorate-general
661 of Research, Environment and Sustainable Development programme, project no. GOCE-CT-2003-
662 505361.

663

664 Jonas Souza would like to thank University of Liverpool for provision of facilities during a year's visit
665 and The Brazilian Council of Technological and Scientific Development (Conselho Nacional de
666 Desenvolvimento Científico e Tecnológico - CNPq, grant number 203959/2018-3) for financial
667 support.

668

669 **REFERENCES**

670 Asadi, H., Shahedi, K., Jarihani, B., Sidle, R.C., 2019. Rainfall-runoff modelling using hydrological
671 connectivity index and artificial neural network approach. Water (Switzerland) 11, 212.
672 https://doi.org/10.3390/w11020212

673 Bordoni, M., Giuseppina Persichillo, M., Meisina, C., Crema, S., Cavalli, M., Bartelletti, C., Galanti, Y.,
674 Barsanti, M., Giannecchini, R., D'Amato Avanzi, G., 2018. Estimation of the susceptibility of a
675 road network to shallow landslides with the integration of the sediment connectivity. Nat.
676 Hazards Earth Syst. Sci. 18, 1735–1758. https://doi.org/10.5194/nhess-18-1735-2018

677 Borselli, L., Cassi, P., Torri, D., 2008. Prolegomena to sediment and flow connectivity in the
678 landscape: A GIS and field numerical assessment. Catena 75, 268–277.
679 https://doi.org/10.1016/j.catena.2008.07.006

680 Bracken, L.J., Croke, J., 2007. The concept of hydrological connectivity and its contribution to
681 understanding runoff-dominated geomorphic systems. Hydrol. Process. 21, 1749–1763.
682 https://doi.org/10.1002/hyp.6313

683 Bracken, L.J., Wainwright, J., Ali, G.A., Tetzlaff, D., Smith, M.W., Reaney, S.M., Roy, A.G., 2013.
684 Concepts of hydrological connectivity: Research approaches, Pathways and future agendas.
685 Earth-Science Rev. https://doi.org/10.1016/j.earscirev.2013.02.001

686 Brierley, G., Fryirs, K., Jain, V., 2006. Landscape connectivity: The geographic basis of geomorphic
687 applications. Area 38, 165–174. https://doi.org/10.1111/j.1475-4762.2006.00671.x

688 Brierley, G.J., Fryirs, K., 1999. Tributary-trunk stream relations in a cut-and-fill landscape: A case
689 study from Wolumla catchment, New South Wales, Australia. Geomorphology 28, 61–73.
690 https://doi.org/10.1016/S0169-555X(98)00103-2

691 Calsamiglia, A., Lucas-Borja, M.E., Fortesa, J., García-Comendador, J., Estrany, J., 2017. Changes in
692 soil quality and hydrological connectivity caused by the abandonment of terraces in a

693 Mediterranean burned catchment. Forests 8, 333. https://doi.org/10.3390/f8090333

694 Calsamiglia, A., Fortesa, J., García-Comendador, J., Lucas-Borja, M.E., Calvo-Cases, A., Estrany, J.,
695 2018a. Spatial patterns of sediment connectivity in terraced lands: Anthropogenic controls of
696 catchment sensitivity. L. Degrad. Dev. 29, 1198–1210. https://doi.org/10.1002/ldr.2840

697 Calsamiglia, A., García-Comendador, J., Fortesa, J., López-Tarazón, J.A., Crema, S., Cavalli, M., Calvo-
698 Cases, A., Estrany, J., 2018b. Effects of agricultural drainage systems on sediment connectivity
699 in a small Mediterranean lowland catchment. Geomorphology 318, 162–171.
700 https://doi.org/10.1016/j.geomorph.2018.06.011

701 Calsamiglia, A., Gago, J., Garcia-Comendador, J., Bernat, J.F., Calvo-Cases, A., Estrany, J., 2020.
702 Evaluating functional connectivity in a small agricultural catchment under contrasting flood
703 events by using UAV. Earth Surf. Process. Landforms 45, 800–815.
704 https://doi.org/10.1002/esp.4769

705 Cammeraat, E.L.H., 2005. RECONDES: Field Protocol version 1.0, in: Hooke, J.M., Sandercock, P.
706 (Eds.), RECONDES. Final Report. University of Portsmouth, p. 100.

707 Cantreul, V., Bielders, C., Calsamiglia, A., Degré, A., 2018. How pixel size affects a sediment
708 connectivity index in central Belgium. Earth Surf. Process. Landforms 43, 884–893.
709 https://doi.org/10.1002/esp.4295

710 Cavalli, M., Trevisani, S., Comiti, F., Marchi, L., 2013. Geomorphometric assessment of spatial
711 sediment connectivity in small Alpine catchments. Geomorphology 188, 31–41.
712 https://doi.org/10.1016/j.geomorph.2012.05.007

713 Cavalli, M., Vericat, D., Pereira, P., 2019. Mapping water and sediment connectivity. Sci. Total
714 Environ. https://doi.org/10.1016/j.scitotenv.2019.04.071

715 Chartin, C., Evrard, O., Laceby, J.P., Onda, Y., Ottlé, C., Lefèvre, I., Cerdan, O., 2017. The impact of
716 typhoons on sediment connectivity: lessons learnt from contaminated coastal catchments of

717 the Fukushima Prefecture (Japan), in: Earth Surface Processes and Landforms. pp. 306–317.
718 https://doi.org/10.1002/esp.4056

719 Chen, J., Yang, S., Li, H., Zhang, B., Lv, J., 2013. Research on geographical environment unit division
720 based on the method of natural breaks (Jenks), in: International Archives of the
721 Photogrammetry, Remote Sensing and Spatial Information Sciences - ISPRS Archives. pp. 47–
722 50. https://doi.org/10.5194/isprsarchives-XL-4-W3-47-2013

723 Cislaghi, A., Bischetti, G.B., 2019. Source areas, connectivity, and delivery rate of sediments in
724 mountainous-forested hillslopes: A probabilistic approach. Sci. Total Environ. 652, 1168–1186.
725 https://doi.org/10.1016/j.scitotenv.2018.10.318

726 Cossart, E., Viel, V., Lissak, C., Reulier, R., Fressard, M., Delahaye, D., 2018. How might sediment
727 connectivity change in space and time? L. Degrad. Dev. 29, 2595–2613.
728 https://doi.org/10.1002/ldr.3022

729 Crema, S., Cavalli, M., 2018. SedInConnect: a stand-alone, free and open source tool for the
730 assessment of sediment connectivity. Comput. Geosci. 111, 39–45.
731 https://doi.org/10.1016/j.cageo.2017.10.009

732 Cucchiaro, S., Cazorzi, F., Marchi, L., Crema, S., Beinat, A., Cavalli, M., 2019. Multi-temporal analysis
733 of the role of check dams in a debris-flow channel: Linking structural and functional
734 connectivity. Geomorphology 345, 106844. https://doi.org/10.1016/j.geomorph.2019.106844

735 de Walque, B., Degré, A., Maugnard, A., Bielders, C.L., 2017. Artificial surfaces characteristics and
736 sediment connectivity explain muddy flood hazard in Wallonia. Catena 158, 89–101.
737 https://doi.org/10.1016/j.catena.2017.06.016

738 Estrany, J., Ruiz, M., Calsamiglia, A., Carriquí, M., García-Comendador, J., Nadal, M., Fortesa, J.,
739 López-Tarazón, J.A., Medrano, H., Gago, J., 2019. Sediment connectivity linked to vegetation
740 using UAVs: High-resolution imagery for ecosystem management. Sci. Total Environ. 671,

1192–1205. https://doi.org/10.1016/j.scitotenv.2019.03.399

Faulkner, H., 2008. Connectivity as a crucial determinant of badland morphology and evolution. Geomorphology 100, 91–103. https://doi.org/10.1016/j.geomorph.2007.04.039

Foerster, S., Wilczok, C., Brosinsky, A., Segl, K., 2014. Assessment of sediment connectivity from vegetation cover and topography using remotely sensed data in a dryland catchment in the Spanish Pyrenees. J. Soils Sediments 14, 1982–2000. https://doi.org/10.1007/s11368-014-0992-3

Franco, V.V., Souza, J.O.P. de, 2019. Conectividade de sedimentos na Bacia Hidrográfica Riacho do Tigre, ambiente semiárido no município de São João do Tigre-PB. GEOUSP Espaço e Tempo 23, 697–711. https://doi.org/10.11606/issn.2179-0892.geousp.2019.151940

Fressard, M., Cossart, E., 2019. A graph theory tool for assessing structural sediment connectivity: Development and application in the Mercurey vineyards (France). Sci. Total Environ. 651, 2566–2584. https://doi.org/10.1016/j.scitotenv.2018.10.158

Fryirs, K.A., Brierley, G.J., Preston, N.J., Kasai, M., 2007a. Buffers, barriers and blankets: The (dis)connectivity of catchment-scale sediment cascades. Catena 70, 49–67. https://doi.org/10.1016/j.catena.2006.07.007

Fryirs, K.A., Brierley, G.J., Preston, N.J., Spencer, J., 2007b. Catchment-scale (dis)connectivity in sediment flux in the upper Hunter catchment, New South Wales, Australia. Geomorphology 84, 297–316. https://doi.org/10.1016/j.geomorph.2006.01.044

Gay, A., Cerdan, O., Mardhel, V., Desmet, M., 2016. Application of an index of sediment connectivity in a lowland area. J. Soils Sediments 16, 280–293. https://doi.org/10.1007/s11368-015-1235-y

Heckmann, T., Cavalli, M., Cerdan, O., Foerster, S., Javaux, M., Lode, E., Smetanová, A., Vericat, D., Brardinoni, F., 2018. Indices of sediment connectivity: opportunities, challenges and limitations. Earth-Science Rev. https://doi.org/10.1016/j.earscirev.2018.08.004

765 Heckmann, T., Schwanghart, W., 2013. Geomorphic coupling and sediment connectivity in an alpine
766 catchment - Exploring sediment cascades using graph theory. Geomorphology 182, 89–103.
767 https://doi.org/10.1016/j.geomorph.2012.10.033

768 Hooke, J., 2003. Coarse sediment connectivity in river channel systems: A conceptual framework and
769 methodology. Geomorphology 56, 79–94. https://doi.org/10.1016/S0169-555X(03)00047-3

770 Hooke, J., Sandercock, P., 2017. Combating Desertification and Land Degradation, SpringerBriefs in
771 Environmental Science. Springer International Publishing, Cham. https://doi.org/10.1007/978-
772 3-319-44451-2

773 Hooke, J., Sandercock, P., 2012. Use of vegetation to combat desertification and land degradation:
774 Recommendations and guidelines for spatial strategies in Mediterranean lands. Landsc. Urban
775 Plan. 107, 389–400. https://doi.org/10.1016/j.landurbplan.2012.07.007

776 Hooke, J.M., 2019. Extreme sediment fluxes in a dryland flash flood. Sci. Rep. 9, 1686.
777 https://doi.org/10.1038/s41598-019-38537-3

778 Hooke, J.M., 2016. Morphological impacts of flow events of varying magnitude on ephemeral
779 channels in a semiarid region. Geomorphology 252, 128–143.
780 https://doi.org/10.1016/j.geomorph.2015.07.014

781 Hooke, J.M., 2006. Human impacts on fluvial systems in the Mediterranean region. Geomorphology
782 79, 311–335. https://doi.org/10.1016/j.geomorph.2006.06.036

783 Koci, J., Sidle, R.C., Jarihani, B., Cashman, M.J., 2020. Linking hydrological connectivity to gully
784 erosion in savanna rangelands tributary to the Great Barrier Reef using structure-from-motion
785 photogrammetry. L. Degrad. Dev. 31, 20–36. https://doi.org/10.1002/ldr.3421

786 Kumar, R., Jain, V., Prasad Babu, G., Sinha, R., 2014. Connectivity structure of the Kosi megafan and
787 role of rail-road transport network. Geomorphology 227, 73–86.
788 https://doi.org/10.1016/j.geomorph.2014.04.031

789 Lana-Renault, N., López-Vicente, M., Nadal-Romero, E., Ojanguren, R., Llorente, J.A., Errea, P.,
790 Regüés, D., Ruiz-Flaño, P., Khorchani, M., Arnáez, J., Pascual, N., 2018. Catchment based
791 hydrology under post farmland abandonment scenarios. Geogr. Res. Lett. 44, 503–534.
792 https://doi.org/10.18172/cig.3475

793 Lesschen, J.P., Cammeraat, L.H., Nieman, T., 2008. Erosion and terrace failure due to agricultural
794 land abandonment in a semi-arid environment. Earth Surf. Process. Landforms 33, 1574–1584.
795 https://doi.org/10.1002/esp.1676

796 Lesschen, J.P., Schoorl, J.M., Cammeraat, L.H., 2009. Modelling runoff and erosion for a semi-arid
797 catchment using a multi-scale approach based on hydrological connectivity. Geomorphology
798 109, 174–183. https://doi.org/10.1016/j.geomorph.2009.02.030

799 Lexartza-Artza, I., Wainwright, J., 2009. Hydrological connectivity: Linking concepts with practical
800 implications. Catena 79, 146–152. https://doi.org/10.1016/j.catena.2009.07.001

801 Lizaga, I., Quijano, L., Palazón, L., Gaspar, L., Navas, A., 2018. Enhancing Connectivity Index to Assess
802 the Effects of Land Use Changes in a Mediterranean Catchment. L. Degrad. Dev. 29, 663–675.
803 https://doi.org/10.1002/ldr.2676

804 Llena, M., Vericat, D., Cavalli, M., Crema, S., Smith, M.W., 2019. The effects of land use and
805 topographic changes on sediment connectivity in mountain catchments. Sci. Total Environ. 660,
806 899–912. https://doi.org/10.1016/j.scitotenv.2018.12.479

807 López-Vicente, M., Álvarez, S., 2018. Influence of DEM resolution on modelling hydrological
808 connectivity in a complex agricultural catchment with woody crops. Earth Surf. Process.
809 Landforms 43, 1403–1415. https://doi.org/10.1002/esp.4321

810 López-Vicente, M., Ben-Salem, N., 2019. Computing structural and functional flow and sediment
811 connectivity with a new aggregated index: A case study in a large Mediterranean catchment.
812 Sci. Total Environ. 651, 179–191. https://doi.org/10.1016/j.scitotenv.2018.09.170

López-Vicente, M., González-Romero, J., Lucas-Borja, M.E., 2020. Forest fire effects on sediment connectivity in headwater sub-catchments: Evaluation of indices performance. Sci. Total Environ. 732, 139206. https://doi.org/10.1016/j.scitotenv.2020.139206

López-Vicente, M., Nadal-Romero, E., Cammeraat, E.L.H., 2017. Hydrological Connectivity Does Change Over 70 Years of Abandonment and Afforestation in the Spanish Pyrenees. L. Degrad. Dev. 28, 1298–1310. https://doi.org/10.1002/ldr.2531

López-Vicente, M., Poesen, J., Navas, A., Gaspar, L., 2013. Predicting runoff and sediment connectivity and soil erosion by water for different land use scenarios in the Spanish Pre-Pyrenees. Catena 102, 62–73. https://doi.org/10.1016/j.catena.2011.01.001

Marchamalo, M., Hooke, J.M., Sandercock, P.J., 2016. Flow and Sediment Connectivity in Semi-arid Landscapes in SE Spain: Patterns and Controls. L. Degrad. Dev. 27, 1032–1044. https://doi.org/10.1002/ldr.2352

Marchi, L., Comiti, F., Crema, S., Cavalli, M., 2019. Channel control works and sediment connectivity in the European Alps. Sci. Total Environ. 668, 389–399. https://doi.org/10.1016/j.scitotenv.2019.02.416

Meerkerk, A.L., van Wesemael, B., Bellin, N., 2009. Application of connectivity theory to model the impact of terrace failure on runoff in semi-arid catchments. Hydrol. Process. 23, 2792–2803. https://doi.org/10.1002/hyp.7376

Messenzehl, K., Hoffmann, T., Dikau, R., 2014. Sediment connectivity in the high-alpine valley of Val Müschauns, Swiss National Park - linking geomorphic field mapping with geomorphometric modelling. Geomorphology 221, 215–229. https://doi.org/10.1016/j.geomorph.2014.05.033

Moreno-de-las-Heras, M., Lindenberger, F., Latron, J., Lana-Renault, N., Llorens, P., Arnáez, J., Romero-Díaz, A., Gallart, F., 2019. Hydro-geomorphological consequences of the abandonment of agricultural terraces in the Mediterranean region: Key controlling factors and landscape

837 stability patterns. Geomorphology. https://doi.org/10.1016/j.geomorph.2019.02.014

838 Nicoll, T., Brierley, G., 2017. Within-catchment variability in landscape connectivity measures in the
839 Garang catchment, upper Yellow River. Geomorphology 277, 197–209.
840 https://doi.org/10.1016/j.geomorph.2016.03.014

841 Ortíz-Rodríguez, A.J., Borselli, L., Sarocchi, D., 2017. Flow connectivity in active volcanic areas: Use of
842 index of connectivity in the assessment of lateral flow contribution to main streams. Catena
843 157, 90–111. https://doi.org/10.1016/j.catena.2017.05.009

844 Ortíz-Rodríguez, A.J., Muñoz-Robles, C., Borselli, L., 2019. Changes in connectivity and hydrological
845 efficiency following wildland fires in Sierra Madre Oriental, Mexico. Sci. Total Environ. 655,
846 112–128. https://doi.org/10.1016/j.scitotenv.2018.11.236

847 Panagos, P., Borrelli, P., Meusburger, K., Alewell, C., Lugato, E., Montanarella, L., 2015. Estimating
848 the soil erosion cover-management factor at the European scale. Land use policy 48, 38–50.
849 https://doi.org/10.1016/j.landusepol.2015.05.021

850 Papaioannou, G., Efstratiadis, A., Vasiliades, L., Loukas, A., Papalexiou, S., Koukouvinos, A., Tsoukalas,
851 I., Kossieris, P., 2018. An Operational Method for Flood Directive Implementation in Ungauged
852 Urban Areas. Hydrology 5, 24. https://doi.org/10.3390/hydrology5020024

853 Persichillo, M.G., Bordoni, M., Cavalli, M., Crema, S., Meisina, C., 2018. The role of human activities
854 on sediment connectivity of shallow landslides. Catena 160, 261–274.
855 https://doi.org/10.1016/j.catena.2017.09.025

856 Recondes, 2017a. Combating land degradation by minimal intervention: The connectivity reduction
857 approach. Practical guidelines.

858 Recondes, 2017b. Conditions for restoration and mitigation of desertified areas in Southern Europe
859 using vegetation. Final Report.

860 Sampson, C.C., Fewtrell, T.J., Duncan, A., Shaad, K., Horritt, M.S., Bates, P.D., 2012. Use of terrestrial
861 laser scanning data to drive decimetric resolution urban inundation models. Adv. Water
862 Resour. 41, 1–17. https://doi.org/10.1016/j.advwatres.2012.02.010

863 Sandercock, P., Hooke, J., 2006. Strategies for reducing sediment connectivity and land degradation
864 in desertified areas using vegetation: The RECONDES project, in: IAHS-AISH Publication. pp.
865 287–294.

866 Sandercock, P.J., Hooke, J.M., 2011. Vegetation effects on sediment connectivity and processes in an
867 ephemeral channel in SE Spain. J. Arid Environ. 75, 239–254.
868 https://doi.org/10.1016/j.jaridenv.2010.10.005

869 Schopper, N., Mergili, M., Frigerio, S., Cavalli, M., Poeppl, R., 2019. Analysis of lateral sediment
870 connectivity and its connection to debris flow intensity patterns at different return periods in
871 the Fella River system in northeastern Italy. Sci. Total Environ. 658, 1586–1600.
872 https://doi.org/10.1016/j.scitotenv.2018.12.288

873 Scorpio, V., Crema, S., Marra, F., Righini, M., Ciccarese, G., Borga, M., Cavalli, M., Corsini, A., Marchi,
874 L., Surian, N., Comiti, F., 2018. Basin-scale analysis of the geomorphic effectiveness of flash
875 floods: A study in the northern Apennines (Italy). Sci. Total Environ. 640–641, 337–351.
876 https://doi.org/10.1016/j.scitotenv.2018.05.252

877 Singh, M., Sinha, R., 2019. Evaluating dynamic hydrological connectivity of a floodplain wetland in
878 North Bihar, India using geostatistical methods. Sci. Total Environ. 651, 2473–2488.
879 https://doi.org/10.1016/j.scitotenv.2018.10.139

880 Sougnez, N., van Wesemael, B., Vanacker, V., 2011. Low erosion rates measured for steep, sparsely
881 vegetated catchments in southeast Spain. Catena.
882 https://doi.org/10.1016/j.catena.2010.08.010

883 Surian, N., Righini, M., Lucía, A., Nardi, L., Amponsah, W., Benvenuti, M., Borga, M., Cavalli, M.,

884 Comiti, F., Marchi, L., Rinaldi, M., Viero, A., 2016. Channel response to extreme floods: Insights
885 on controlling factors from six mountain rivers in northern Apennines, Italy. Geomorphology
886 272, 78–91. https://doi.org/10.1016/j.geomorph.2016.02.002

887 Tarolli, P., Cavalli, M., Masin, R., 2019. High-resolution morphologic characterization of conservation
888 agriculture. Catena 172, 846–856. https://doi.org/10.1016/j.catena.2018.08.026

889 Tiranti, D., Crema, S., Cavalli, M., Deangeli, C., 2018. An integrated study to evaluate debris flow
890 hazard in alpine environment. Front. Earth Sci. 6, 60. https://doi.org/10.3389/feart.2018.00060

891 Trimble, S.W., 1983. A sediment budget for Coon Creek basin in the Driftless Area, Wisconsin, 1853-
892 1977. Am. J. Sci. 283, 454–474. https://doi.org/10.2475/ajs.283.5.454

893 Walling, D.E., 1983. The sediment delivery problem. J. Hydrol. 65, 209–237.
894 https://doi.org/10.1016/0022-1694(83)90217-2

895 Wohl, E., 2017. Connectivity in rivers. Prog. Phys. Geogr. 41, 345–362.
896 https://doi.org/10.1177/0309133317714972

897 Wohl, E., Brierley, G., Cadol, D., Coulthard, T.J., Covino, T., Fryirs, K.A., Grant, G., Hilton, R.G., Lane,
898 S.N., Magilligan, F.J., Meitzen, K.M., Passalacqua, P., Poeppl, R.E., Rathburn, S.L., Sklar, L.S.,
899 2019. Connectivity as an emergent property of geomorphic systems. Earth Surf. Process.
900 Landforms 44, 4–26. https://doi.org/10.1002/esp.4434

901 Zanandrea, F., Michel, G.P., Kobiyama, M., Cardozo, G.L., 2019. Evaluation of different DTMs in
902 sediment connectivity determination in the Mascarada River Watershed, southern Brazil.
903 Geomorphology 332, 80–87. https://doi.org/10.1016/j.geomorph.2019.02.005

904 Zhao, G., Gao, P., Tian, P., Sun, W., Hu, J., Mu, X., 2020. Assessing sediment connectivity and soil
905 erosion by water in a representative catchment on the Loess Plateau, China. CATENA 185,
906 104284. https://doi.org/10.1016/j.catena.2019.104284

907 Zingaro, M., Refice, A., Giachetta, E., D'Addabbo, A., Lovergine, F., De Pasquale, V., Pepe, G.,
908 Brandolini, P., Cevasco, A., Capolongo, D., 2019. Sediment mobility and connectivity in a
909 catchment: A new mapping approach. Sci. Total Environ. 672, 763–775.
910 https://doi.org/10.1016/j.scitotenv.2019.03.461

911

912

913 **Figures**

914 Fig.1 Maps of a) the location, b) relief, and c) land use, of the study sub-catchment

915 Fig. 2 a) Orthophoto mosaic from drone imagery, and locations of key features ,- the blue arrow
916 indicates the position and direction of the image in b) ; b) panoramic photography of the study area;
917 c) photographs of typical erosional and deposition features: clockwise: 1. Flow off track, 2. rill in
918 field, 3.old breach, 4. flow through and downstream of embankment, 5. upstream of the
919 embankment, 6. sedimentation in flow pathway, 7. pathways and sedimentation in terraces, 8. rill
920 from track

921 Fig. 3 Field mapping: a) compilation of sources, pathways and sinks, 2004-2008 (after Marchamalo
922 et al., 2016; Hooke and Sandercock, 2017); b) Major rills mapped on 10 dates, 2008-2020.

923 Fig.4 IC histogram curve of Connectivity Index values for Cárcavo watershed generated by three
924 models with differing weighting factors: Red-RI; Green - n; Blue - C factor.

925 Fig. 5: Examples of IC models showing the differences produced by the two slope algorithms on very
926 steep embankments – slope angle over 1 m/m. Top: Model without slope limit. Bottom: Model with
927 slope limit of 1 m/m.

928 Fig. 6 Whole catchment compilation in the drone mosaic and showing the sub-areas in Figs 6-10. 1:
929 Slope angle. 2/3/4: IC models with different Weighting factors. “C” – C-factor. “n” – manning
930 roughness coefficient. “RI” – Roughness index.

931 Fig. 7 Area2 – Artificial pipe (culvert) and track area

932 Fig. 8 Area 3 – Natural upland area and main track

933 Fig. 9 Area 4 – Terraced area in main drainage line. Y indicates the position of the former main
934 drainage line; Z is the position of a pre-existing embankment breach.

935

936 Fig. 10 Area 5 – Terraced area with varying types and density of crop trees and degree of ploughing

937 Fig. 11 Area 6 – Central drainage area with complex embankments

938 Fig. 12 Sedimentation areas in February 2019; a) Drone photograph, b) ground photograph.

939 Features have been influenced by some management actions.

940

941

942

943 Table 1: Values of C-factor (based on Panagos et al., 2015) and of Manning's n roughness coefficient

944 (based on Persichillo et al., 2018; Zanandrea et al., 2019) parameters

Land Use classes	W – C Factor	W - Mannings n Roughness Values
Tillage	0.9	0.95
Road	0.85	0.95
Bare soil	0.8	0.95
Olive	0.241	0.8
Almond	0.296	0.8
Grass	0.25	0.75
Bushes	0.04	0.65
Trees	0.006	0.6

945

946

947

948 Table 2: Connectivity classes on very steep slope areas (over 1 m/m); Bor – Borselli 2008-
949 without slope limit, Cav – Cavalli 2013 –slope limit of 1 m/m; "C" – C-factor, "n" – manning
950 roughness coefficient. "RI" – Roughness index (Cavalli 2013).

951

952

		MODELS					
		Bor_C	**Cav_C**	**Bor_RI**	**Cav_RI**	**Bor_n**	**Cav_n**
CONNECTIVITY CLASSES	**1**	0.1%	0.2%	0.0%	0.0%	0.0%	0.0%
	2	14.3%	20.5%	0.0%	0.0%	0.0%	0.0%
	3	10.2%	5.7%	0.0%	0.0%	0.0%	0.0%
	4	12.0%	14.5%	0.0%	0.0%	0.1%	0.1%
	5	22.4%	21.0%	0.0%	0.1%	1.8%	4.9%
	6	13.5%	12.7%	0.9%	1.2%	36.5%	47.2%
	7	11.1%	9.8%	17.4%	21.1%	40.0%	29.6%
	8	8.5%	8.6%	47.2%	52.5%	17.6%	15.6%
	9	7.1%	6.7%	30.1%	23.8%	4.0%	2.6%
	10	0.8%	0.4%	4.4%	1.3%	0.0%	0.0%
	MODELS WITH GROUPED CLASSES						
		Bor_C	**Cav_C**	**Bor_RI**	**Cav_RI**	**Bor_n**	**Cav_n**
	Low (1-3)	24.5%	26.4%	0.0%	0.0%	0.0%	0.0%
	Medium (4-7)	59.1%	57.9%	18.3%	22.3%	78.4%	81.7%
	High (8-10)	16.4%	15.7%	81.7%	77.7%	21.6%	18.2%

953

954

955 Table 3: Summary table of statistical differences of grouped connectivity classes between

956 the indices for the whole study catchment (1) and each sub-area (2-6).

957

	MODELS																	
	1_C	**1_n**	**1_RI**	**2_C**	**2_n**	**2_RI**	**3_C**	**3_n**	**3_RI**	**4_C**	**4_n**	**4_RI**	**5_C**	**5_n**	**5_RI**	**6_C**	**6_n**	**6_RI**
low	21.2%	29.6%	34.7%	24.2%	22.0%	25.7%	17.8%	10.9%	11.4%	8.8%	18.8%	25.7%	23.3%	49.1%	58.2%	13.0%	25.9%	32.5%
medium	64.8%	61.6%	53.2%	58.3%	71.9%	69.0%	68.9%	76.6%	60.5%	74.9%	67.0%	57.9%	69.4%	45.4%	35.9%	80.2%	67.5%	58.3%
high	14.0%	8.8%	12.1%	17.5%	6.1%	5.3%	13.3%	12.5%	28.1%	16.3%	14.3%	16.4%	7.3%	5.5%	6.0%	6.8%	6.6%	9.3%

958

959 Fig.1 Maps of a) the location, b) relief, and c) land use, of the study sub-catchment

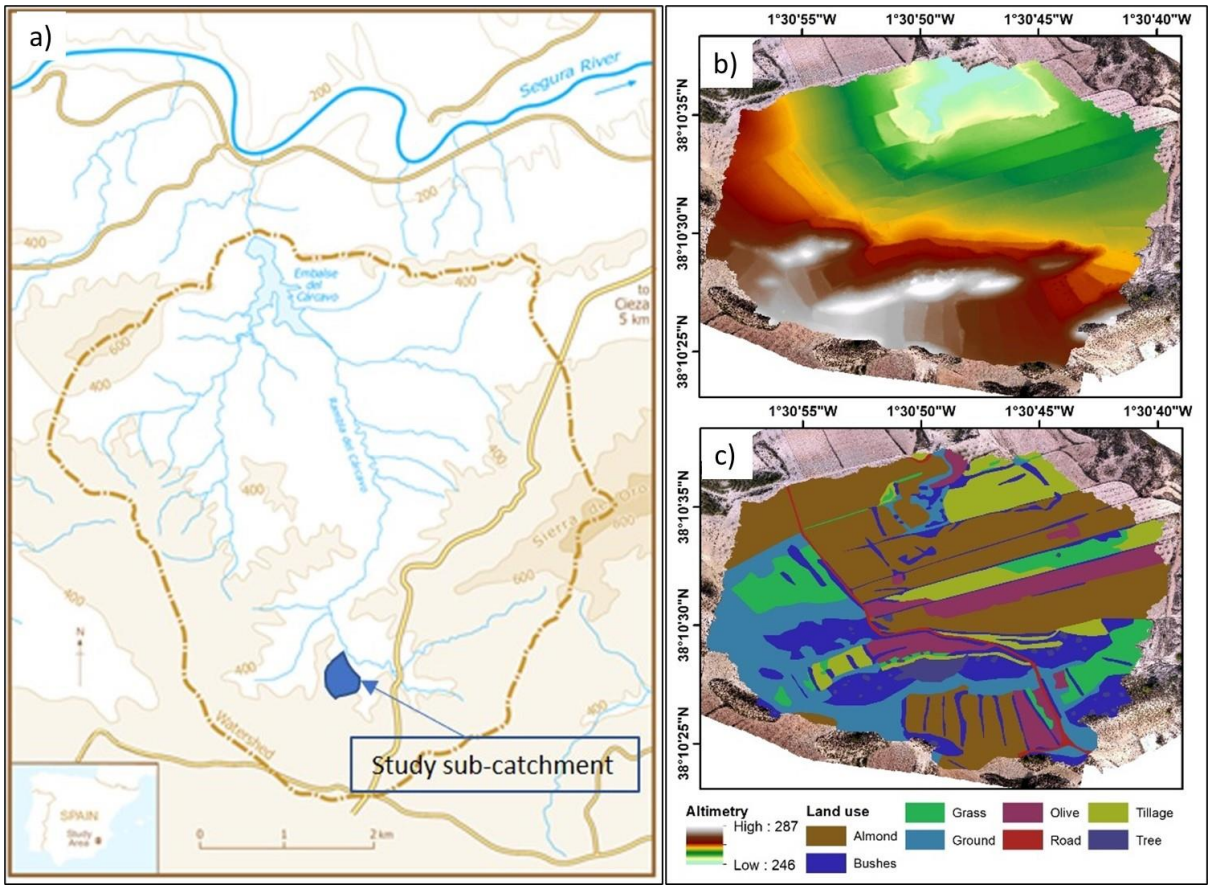

960

961

962

963

964

965 Fig. 2 a) Orthophoto from drone imagery and locations of key features - the blue arrow indicates
966 the position and direction of the image in b) ; b) panoramic photography of the study area; c)
967 photographs of typical erosional and deposition features; clockwise: 1. Flow off track, 2. rill in field,
968 3.old breach, 4. flow through and downstream of embankment, 5. upstream of the embankment, 6.
969 sedimentation in flow pathway, 7. pathways and sedimentation in terraces, 8. rill from track

970

971

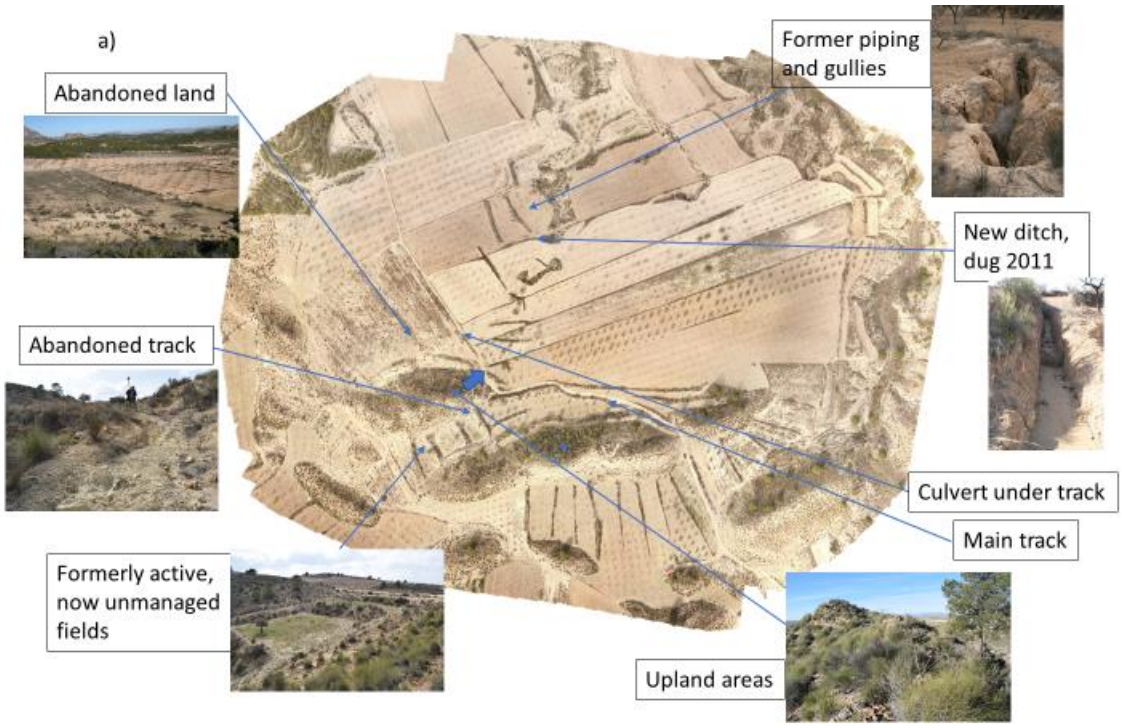

972

973

974

975 Fig.3 Field mapping: a) compilation of sources, pathways and sinks, 2004-2008 (after Marchamalo et
976 al, 2016; Hooke and Sandercock, 2017); b) Major rills mapped on 10 dates, 2008-2020.

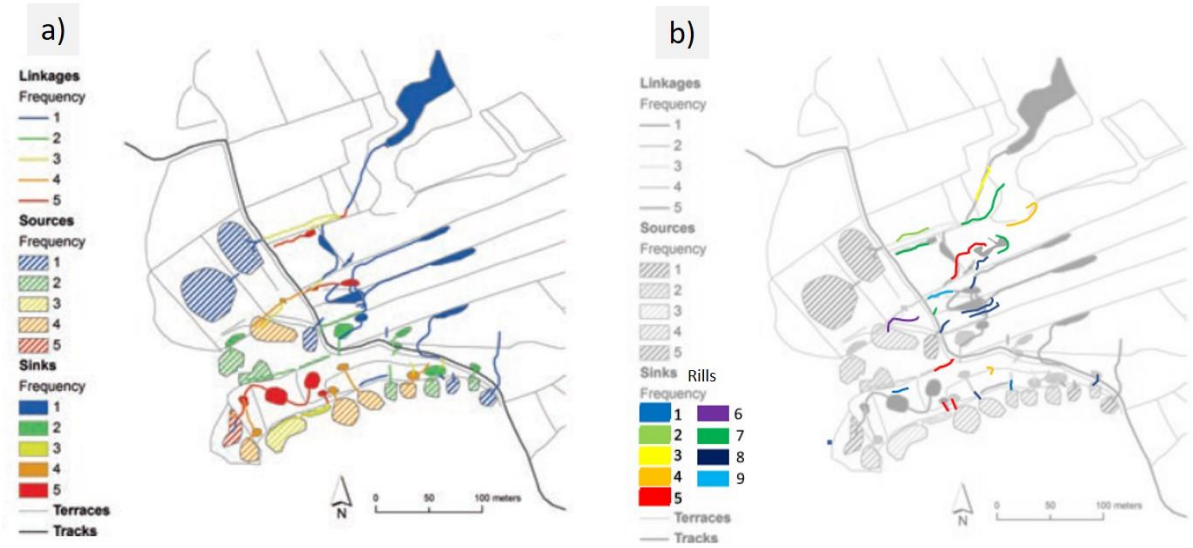

977

978

979

980

981

982

983

984

985

986 Fig.4 IC histogram curve of Connectivity Index values for Cárcavo watershed generated by three

987 models with differing weighting factors: Red - RI; Green - n; Blue - C factor.

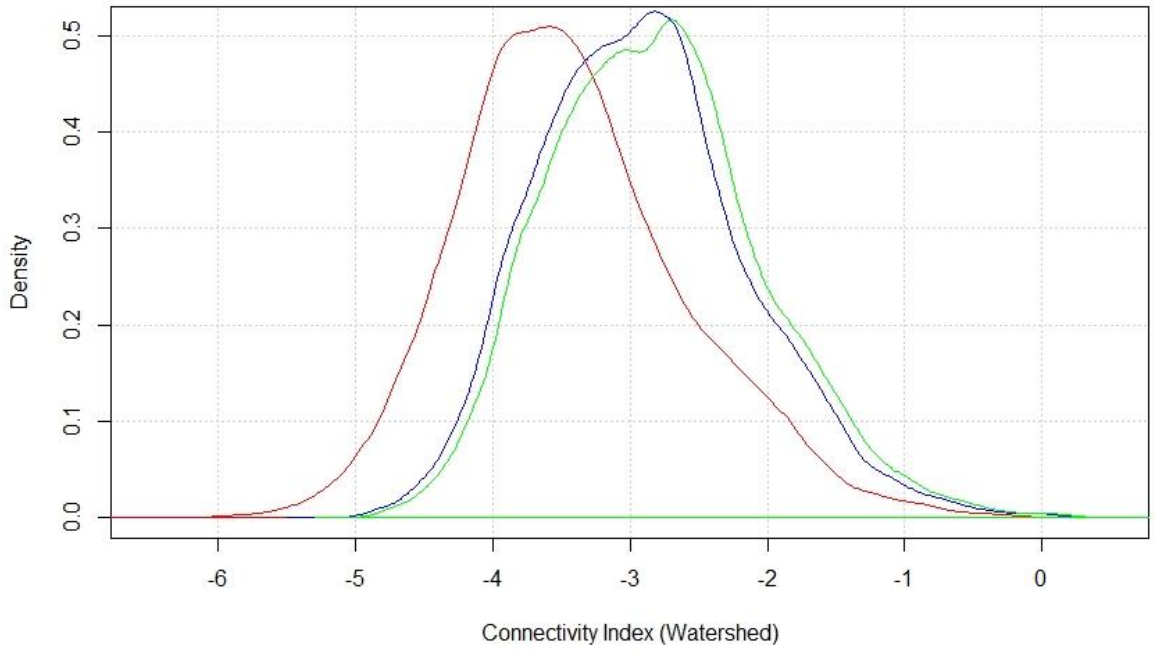

988

989

990

991 Fig. 5: IC models focusing on very steep embankments – slope angle over 1 m/m. Top: Model
992 without slope limit. Bottom: Model with slope limit of 1 m/m.

993

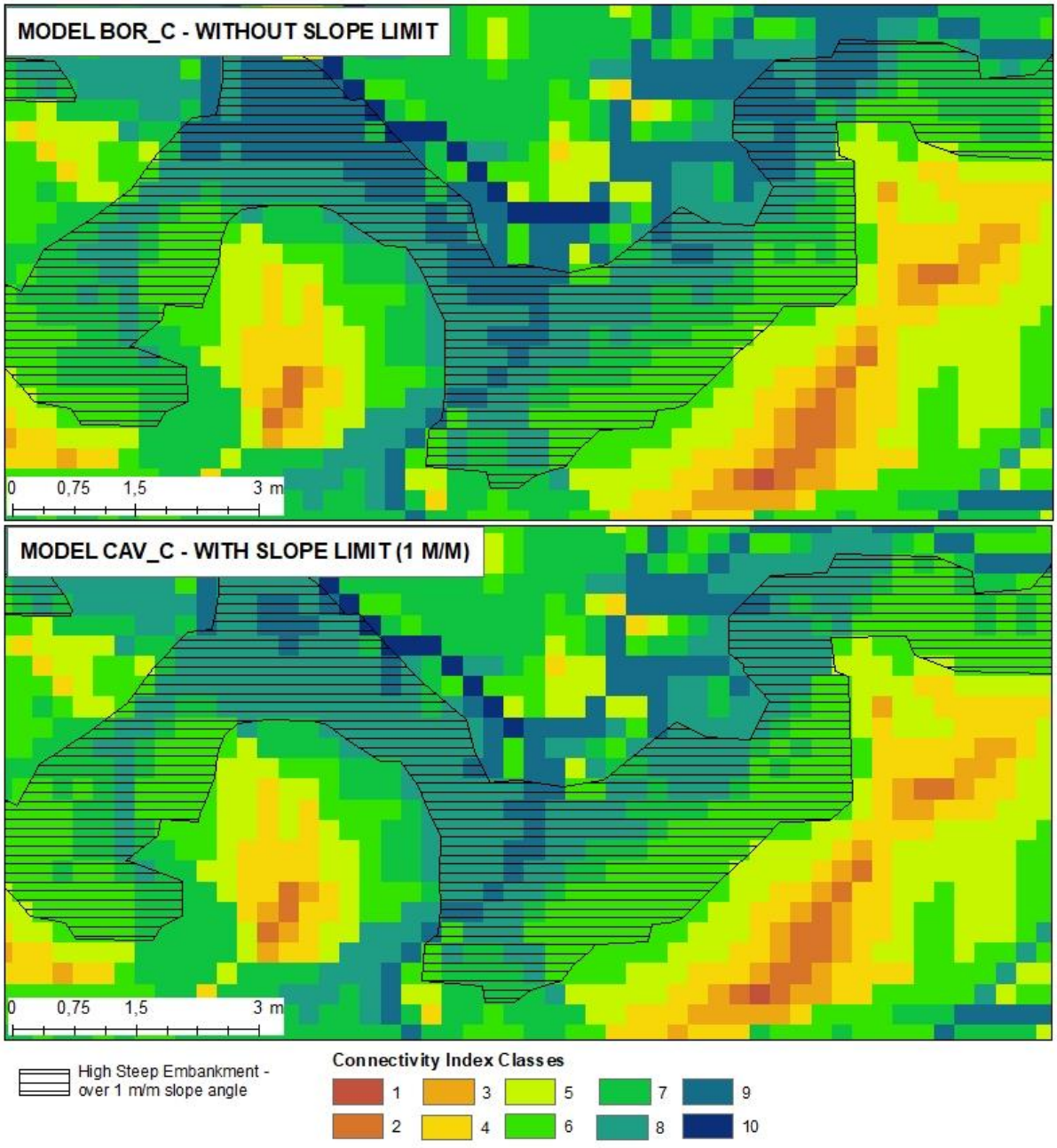

994

995

996

997

998 Fig. 6 Whole catchment compilation but also showing the sub-areas on the drone mosaic. 1: Slope
999 angle. 2/3/4: IC models with different Weighting factors. “C” – C-factor. “n” – manning roughness
1000 coefficient. “RI” – Roughness index.

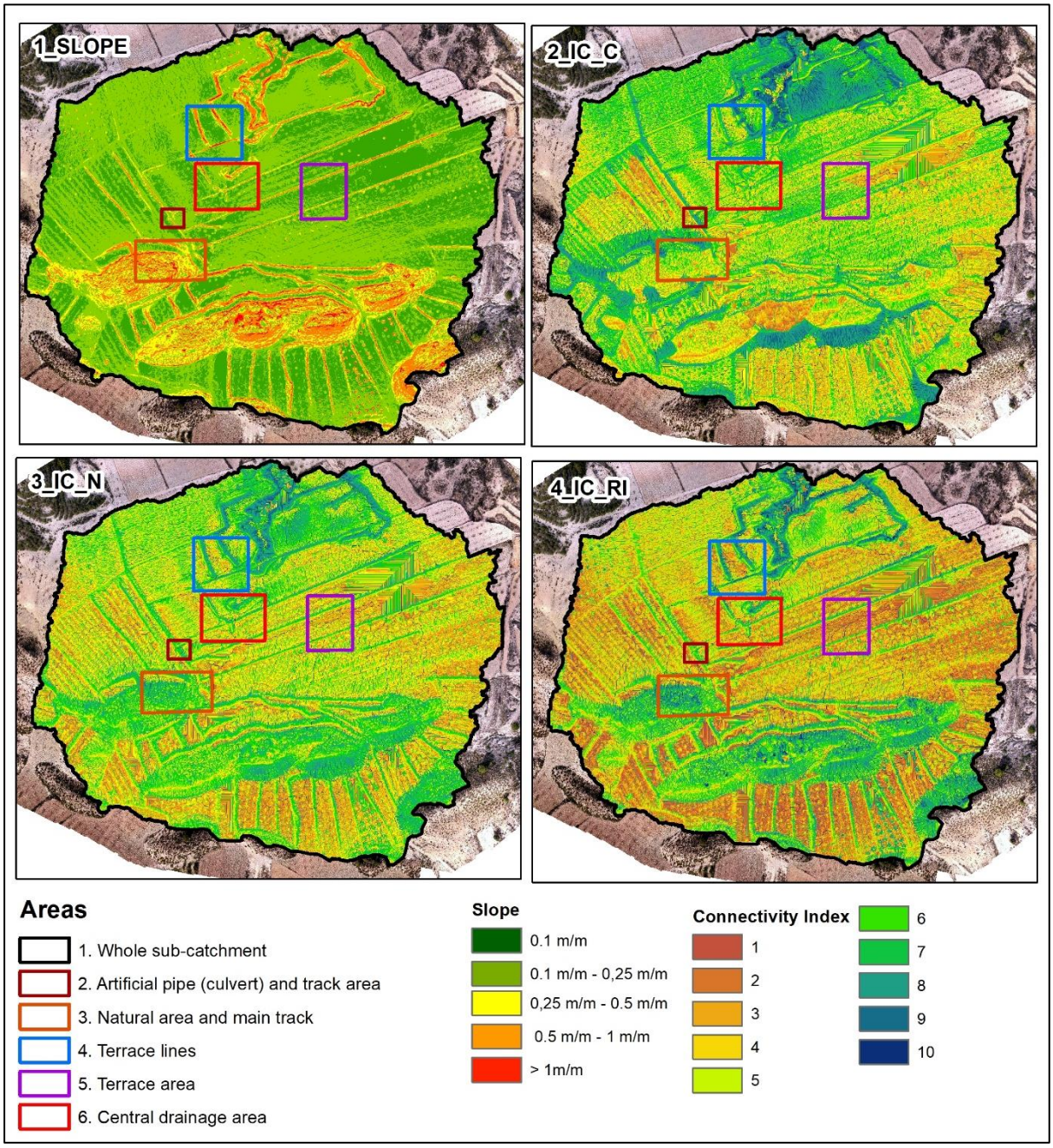

1001

1002 Fig. 7 Area 2 – Artificial pipe (culvert) and track area

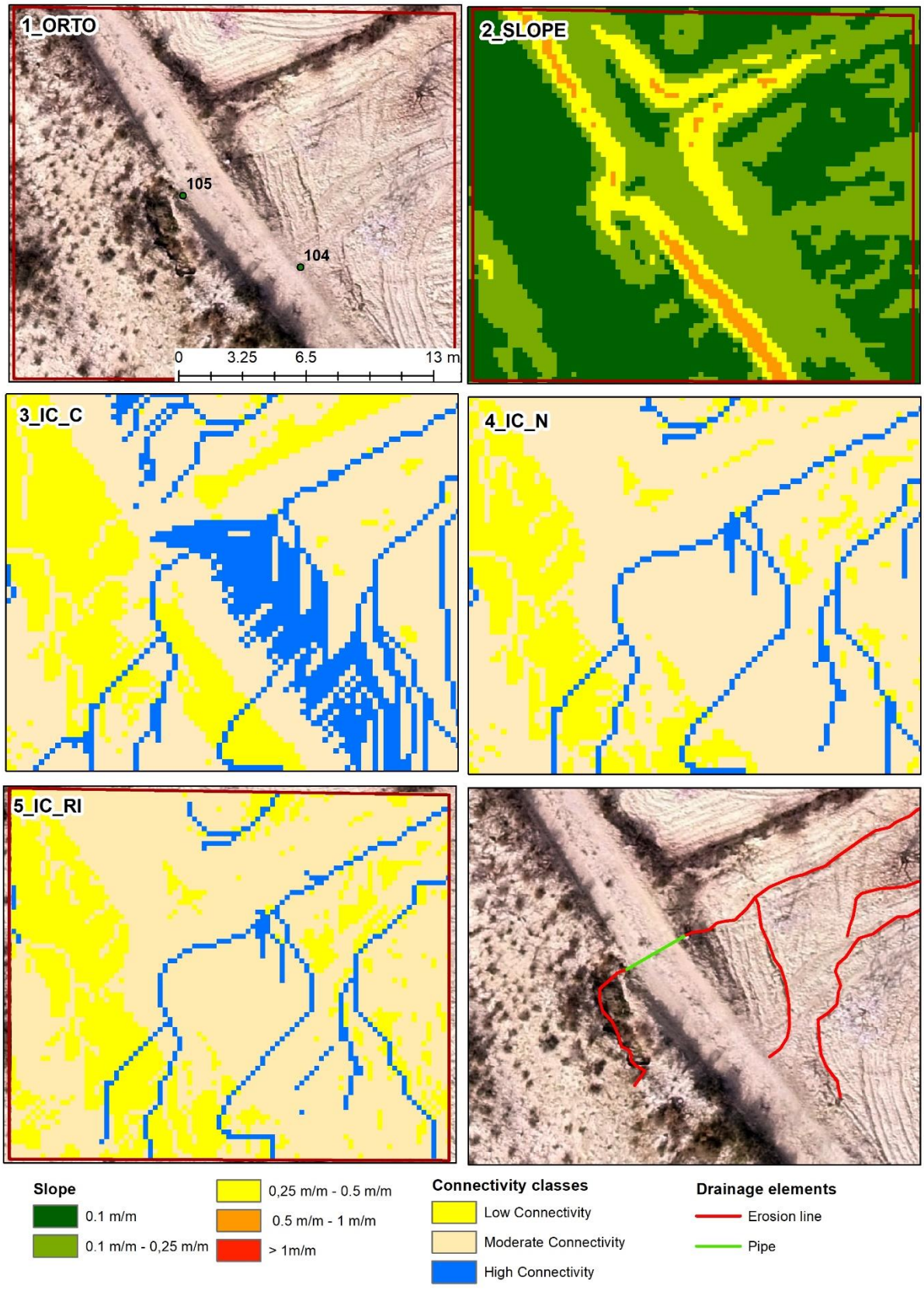

1003

1004 Fig. 8 Area 3 – Natural upland area and main track

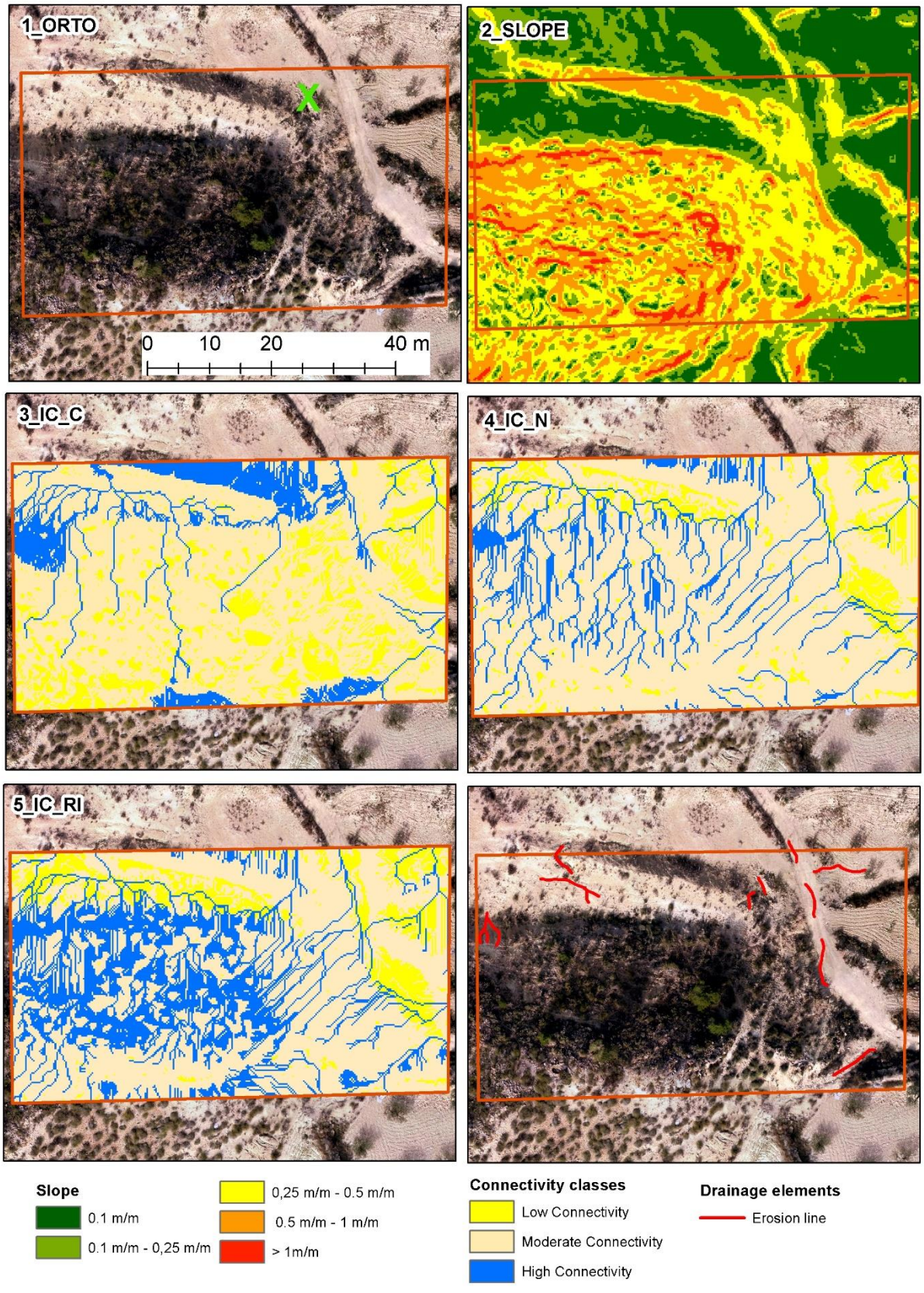

1005

Fig. 9 Area 4 – Terraced area in main drainage line. Y indicates the position of the former main drainage line; Z is the position of a pre-existing embankment breach.

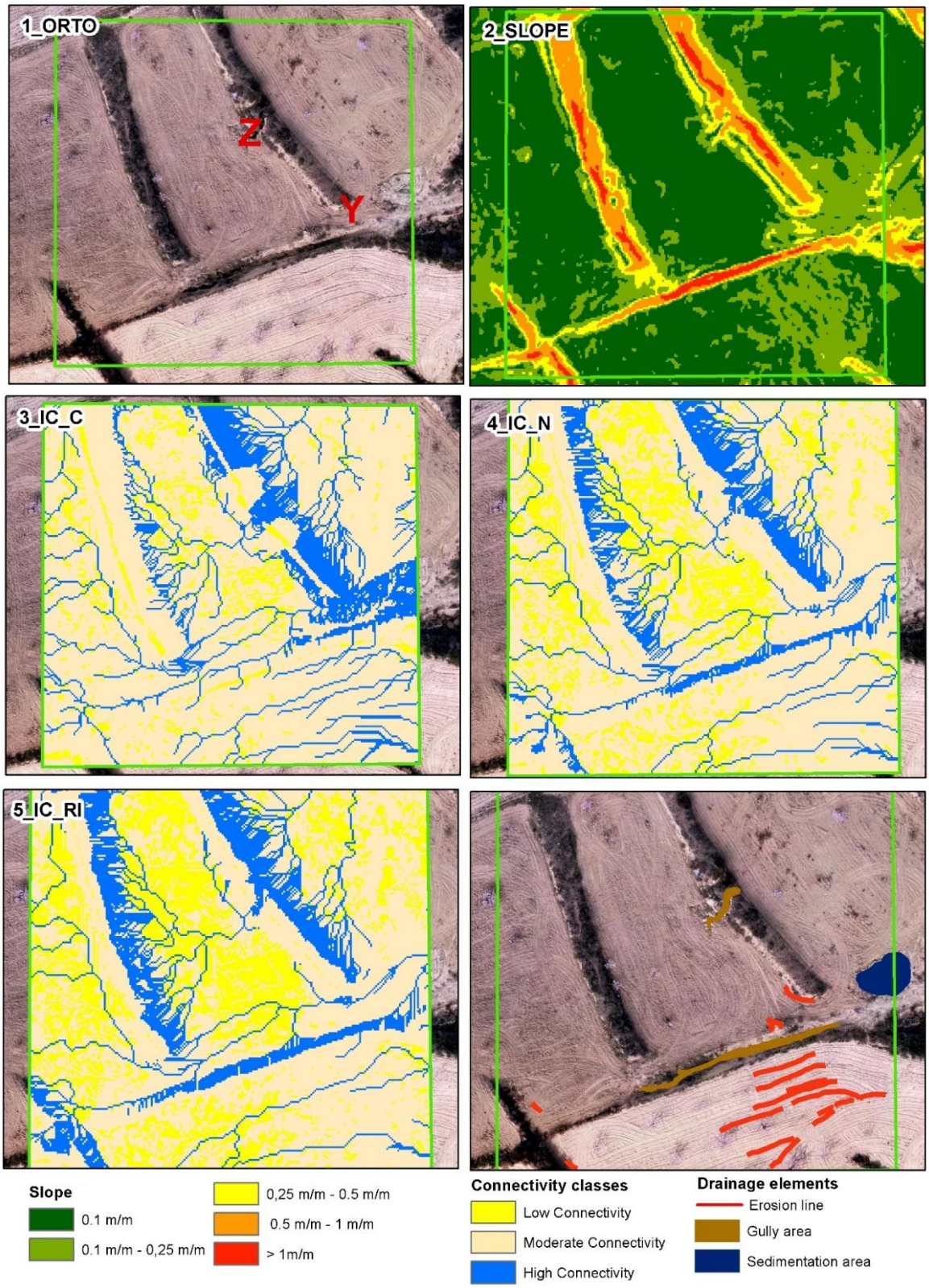

1009 Fig. 10 Area 5 – Terraced area with varying types and density of crop trees and degree of ploughing

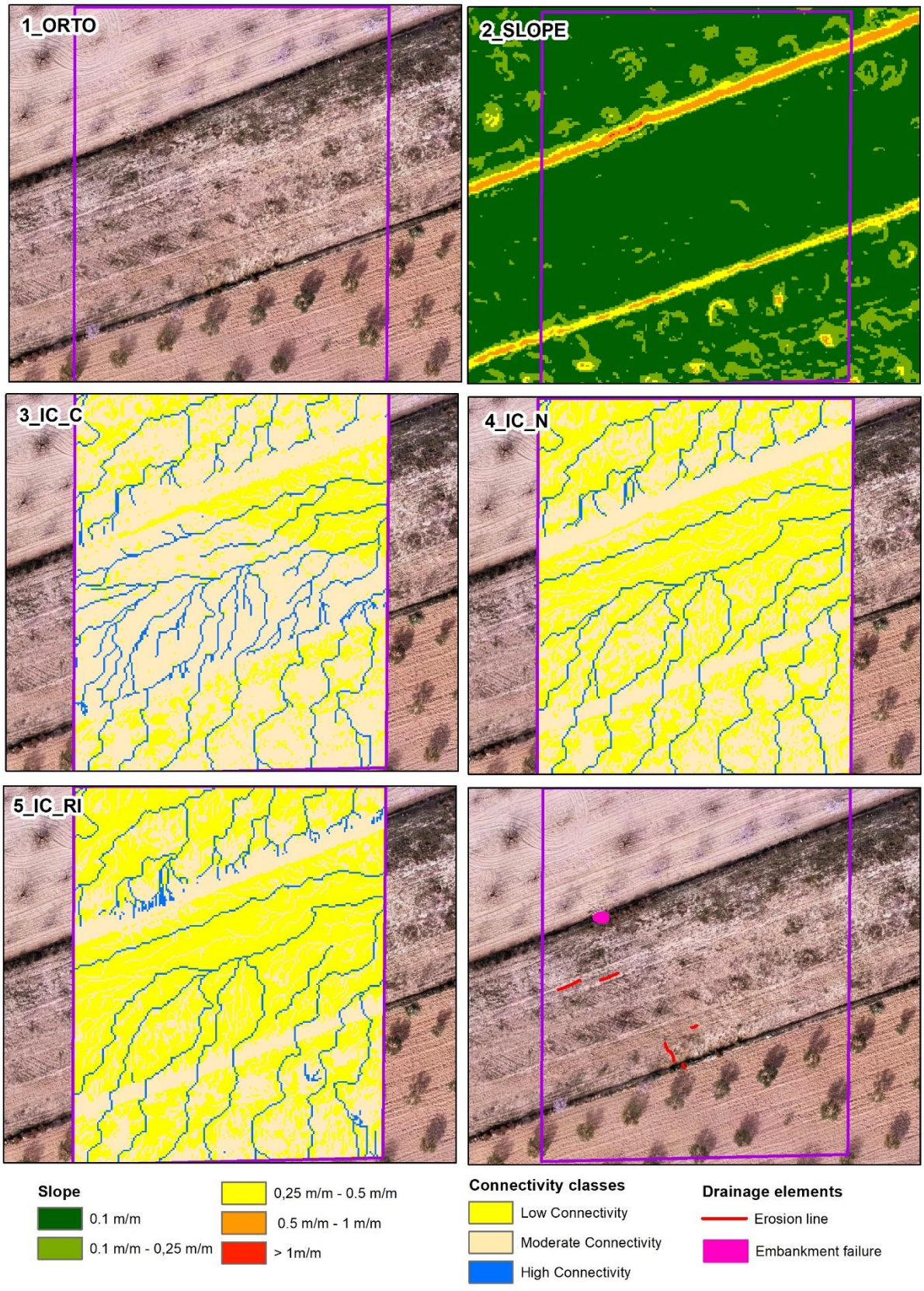

1010

1011 Fig. 11 Area 6 – Central drainage area with complex embankments

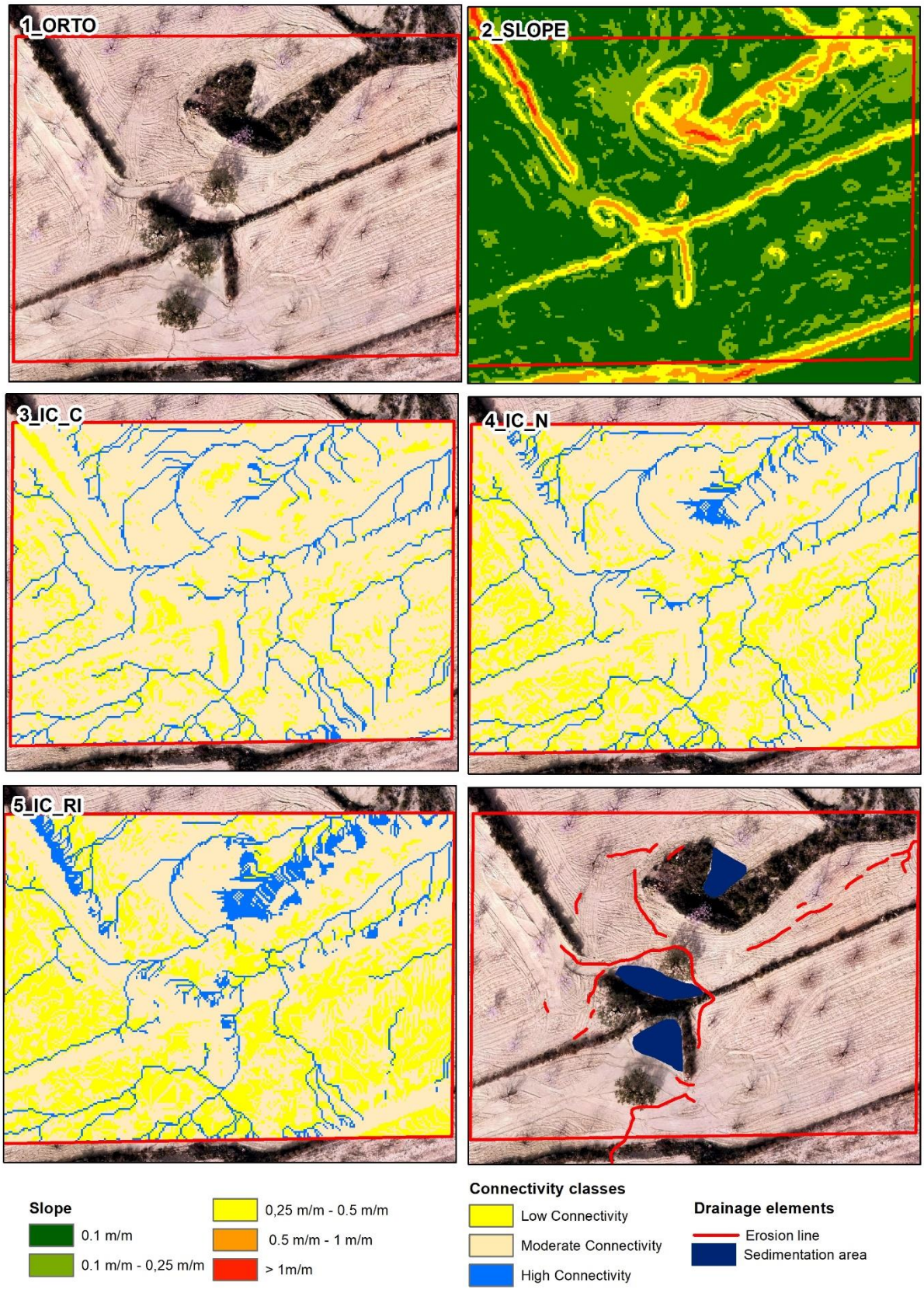

1012

1013

1014 Fig. 12 Sedimentation areas in February 2019; a) Drone photograph, b) ground photograph.

1015 Features have been influenced by some management actions.

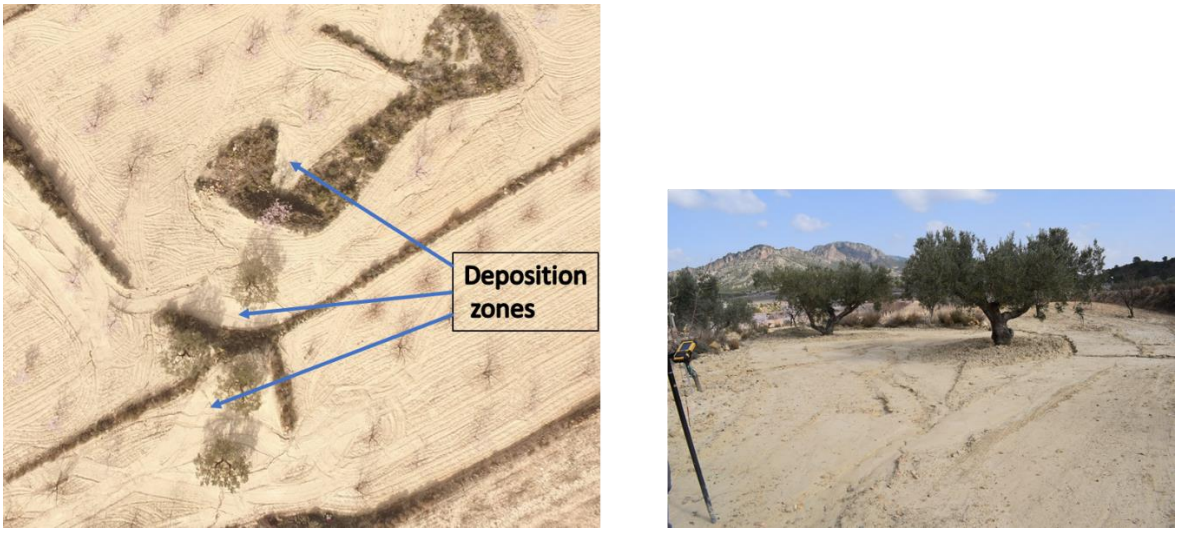

1016